[AMERICAN JOURNAL OF SCIENCE, VOL. 283, SEPTEMBER, 1983, P. 684-721]

GEOMETRY AND KINEMATICS OF FAULT-BEND FOLDING

JOHN SUPPE

Department of Geological and Geophysical Sciences,
Princeton University, Princeton, New Jersey 08544

ABSTRACT. Since the initial study of folds in the hanging wall of the Pine Mountain thrust sheet in the southern Appalachians 50 yrs ago by J. L. Rich, it has become clear that many map-scale folds in sedimentary sequences are formed by the bending of fault blocks as they ride over non-planar fault surfaces. These structures, here called *fault-bend folds*, include "reverse-drag" or "rollovers" associated with normal faults that flatten with depth and the bending of thrust sheets as they ride over steps in decollement. This paper presents a number of geometric and kinematic properties of parallel fault-bend folds, the most important of which is a relationship between fault shape and fold shape for sharp bends in faults. These relationships are useful tools for developing internally consistent cross sections in areas of suspected fault-bend folding, particularly in fold-and-thrust belts.

INTRODUCTION

Many large-scale folds that have formed at shallow crustal levels, above the brittle-plastic transition, have origins that are intimately related to slip on adjacent faults. The important classes of fault-related folding include: (1) buckling caused by compression above a bedding-plane decollement, (2) fault-bend folding caused by bending of a fault-block as it rides over a non-planar fault surface, and (3) fault-propagation folding, caused by compression in front of a fault tip during fault propagation. Because of the shallow-level non-plastic nature of this folding, layer thickness is commonly preserved during deformation, that is, the folding is parallel. This report presents a number of useful geometric and kinematic properties of parallel fault-bend folding. A few examples of their application to real structures are included, many more are published elsewhere together with abbreviated fragments of this theory (Suppe, 1979, 1980a, b; Suppe and Namson, 1979; Namson, 1981).

FAULT-BEND FOLDING

If a fault surface is not planar there must be distortion within at least one of the fault blocks as they slip past one another. The distortion develops because the two blocks remain in tight contact along the fault surface during slip, the rocks not being strong enough to support large voids. If the rocks are layered they may fold in response to riding over a bend in a fault. We call this mechanism of folding *fault-bend folding*. This mechanism is well known in fold-and-thrust belts associated with steps in decollement, in so-called "reverse drag" associated with flattening normal faults (fig. 1), and in "flower structures" associated with bends in strike-slip faults. Fault-bend folding is closely related geometrically to

folding of preexisting faults and refraction of axial surfaces across angular unconformities (fig. 1).

This report presents an idealized two-dimensional geometric description of fault-bend folding, which has applications to all these phenomena (fig. 1). But the emphasis here will lie almost entirely with folds produced by thrust faults and their imbrications. Several sections on applications illustrate the quantitative use of the theory to decipher subsurface map-scale structure in fold-and-thrust belts.

FOLDING DUE TO A SIMPLE RAMP IN DECOLLEMENT HORIZON

Thrust faults do not run forever along a single bedding-plane decollement. The thrust normally steps up in the direction of slip to a higher decollement or to the land surface. As the thrust sheet rides over the bends in the fault it must fold. This fact was clearly perceived by Rich (1934), who applied the concept of fault-bend folding to the interpretation of folds in the Pine Mountain thrust sheet of the southern Appalachians (fig. 2). Rich realized that the Powell Valley anticline is the result of a ramp in decollement of the Pine Mountain thrust from the Lower Cambrian Rome Formation to the Devonian Chattanooga Shale. Analogous folding due to ramps in decollement, both across and along strike, is now widely recognized in many fold-and-thrust belts (for example, Rodgers, 1950; Douglas, 1950; Laubscher, 1965; Gwinn, 1970; Harris, 1970; Perry, Harris, and Harris, 1979; Roedder, Gilbert, and Witherspoon, 1978; Suppe, 1976, 1980a, b; Suppe and Namson, 1979).

The kinematics of fault-bend folding caused by a simple step in decollement along a thrust fault are illustrated in figure 3. Points *X* and *Y*,

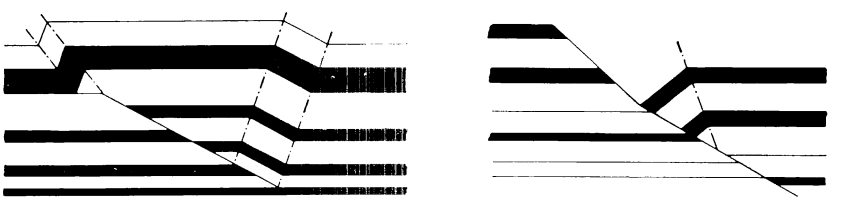

A. Step in decollement on thrust fault. B. Reverse drag on flattening normal faults.

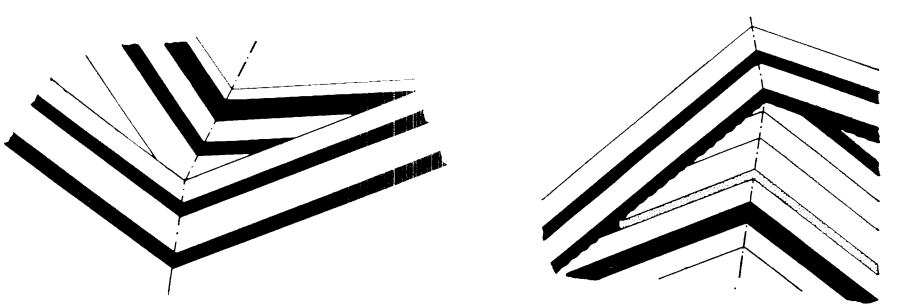

C. Folding of faults. D. Folding of angular unconformities.

Fig. 1. Examples of some common types of fault-bend folds (A-C) and the geometrically related structure of a folded angular unconformity (D).

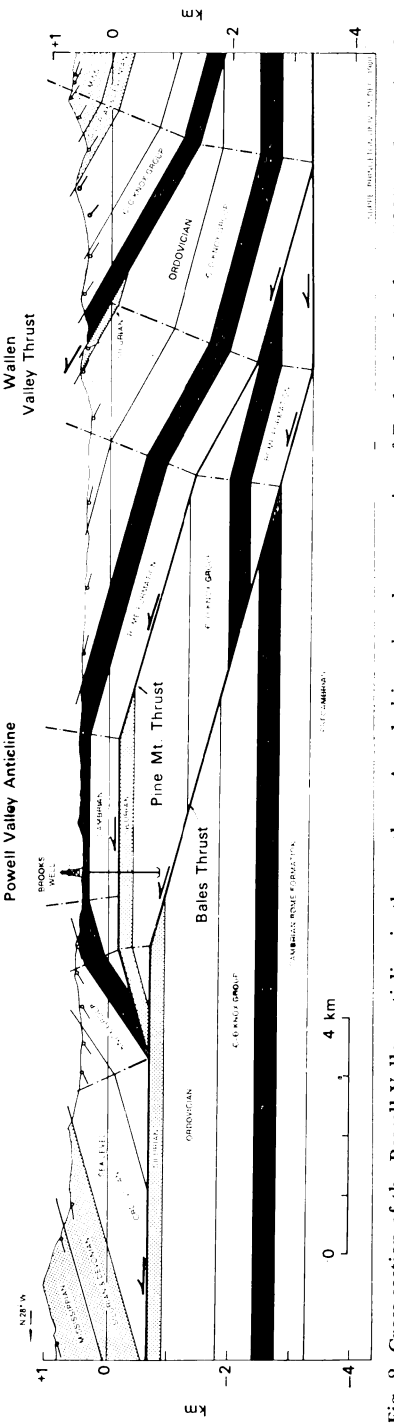

Fig. 2. Cross section of the Powell Valley anticline in the southern Appalachians, based on mapping of Englund and others (1961) and Harris (1962).

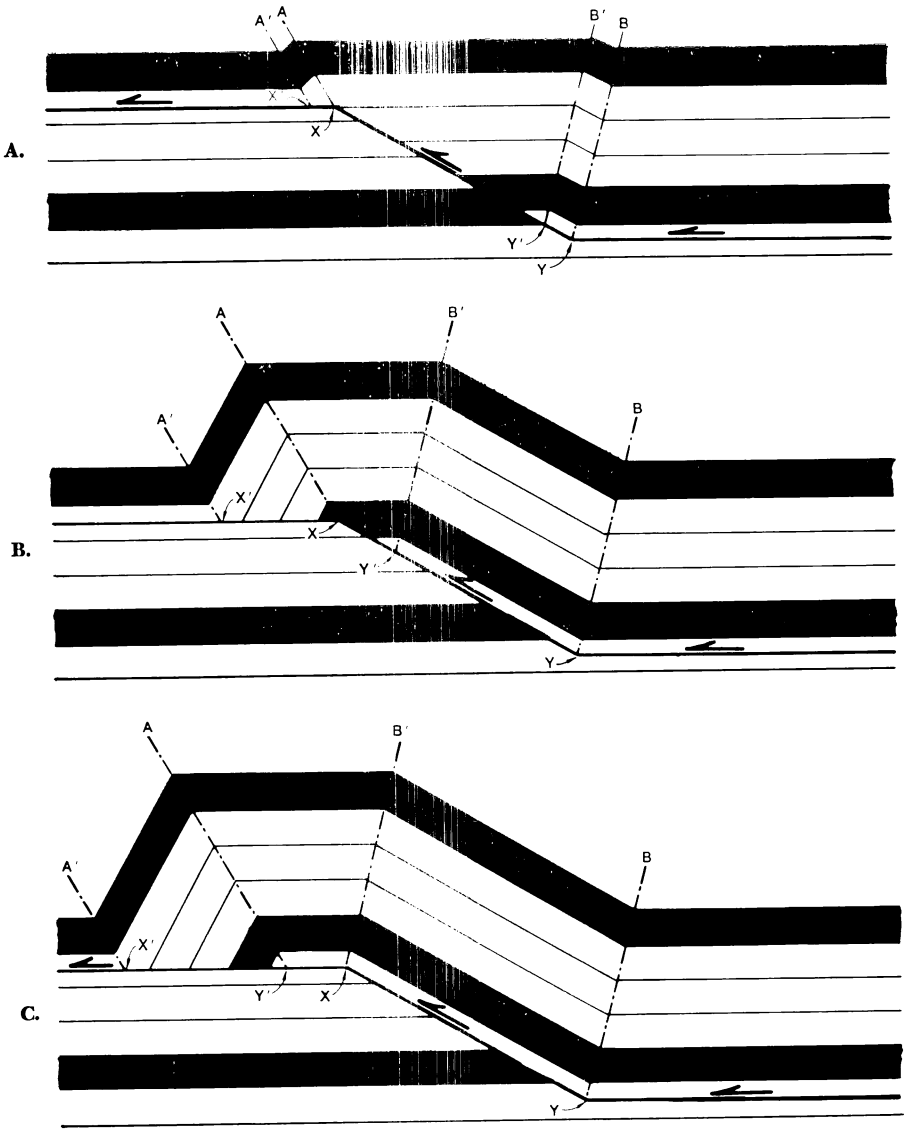

Fig. 3. Kinematic development of fault-bend folds in response to a simple step in decollement (after Suppe and Namson, 1979).

which are lines in 3-dimensions, bound the cross-cutting fault segment in the foot-wall block; points X' and Y' bound the cross-cutting segment of the hanging-wall block. Note that the folds are confined to the hanging-wall block. Axial surfaces A and B terminate along the fault at points (lines) X and Y in the foot-wall block; similarly axial surfaces A' and B' terminate along the fault at points (lines) X' and Y' in the hanging-wall block.

According to the simple geometry of figure 3, two kink bands, A-A' and B-B', form at the instant of initiation of slip. As slip continues, both kink bands grow in width, and the structural relief increases. Note that the slip is not constant along the fault but decreases about 60 percent on the left-hand side, because slip is taken up in kink band A-A'.

Axial surfaces A and B, associated with points X and Y in the foot-wall block of figure 3, remain fixed with respect to the foot-wall block; the beds of the hanging-wall block roll through these two axial surfaces as slip proceeds. In contrast, axial surfaces A' and B', which terminate at points X' and Y' in the hanging-wall block, are fixed in the hanging-wall beds and move with the thrust sheet.

The kinematics are a bit more complex, however, because when point Y' reaches point X, axial surface B' suddenly stops moving with the hanging wall and becomes fixed with respect to the foot wall at point X. At the same instant axial surface A is released from point X in the foot wall and begins to move with point Y' in the hanging wall. When Y' reaches point X the kink bands A-A' and B-B' cease to grow, although rocks still roll through axial surfaces B and B'.

Actual fault-bent folds may not develop precisely as shown diagrammatically in figure 3, because the kinematic details depend on the mechanical properties of the layers and the way in which the forces are applied. The drawings in figure 3 were constructed with the assumptions of (1) preservation of layer thickness, measured normal to bedding, (2) no net distortion where the layers are horizontal, and (3) conservation of bed length. Inclined layers have undergone only layer-parallel slip. We call this set of three assumptions *parallel behavior* in the following discussion.

Many fault-bend folds in unmetamorphosed sedimentary rocks are found to obey the three assumptions of parallel behavior; for example, map, well, and seismic data from the Pakuashan anticline in the Neogene basin of western Taiwan (fig. 4) can be fit to a cross section satisfying the assumptions. The cross section of the Pine Mountain thrust sheet (fig. 2) also obeys the assumptions of parallel behavior.

In most of the following discussion we assume parallel behavior but emphasize that many cases can be found for which the assumptions are invalid, for example in rocks that exhibit slaty cleavage. We are not developing a mechanical theory of fault-bend folding but rather a geometric and kinematic description of a specific material behavior known to be closely approximated in some fault-bend folds, such as the Pine Mountain thrust sheet (fig. 2). The usefulness of the theory comes from its combination of simplicity and rather wide applicability. Similar, but more com-

plex, theories can be formulated to deal with modes of deformation other than parallel behavior. The mode of deformation must be determined by field and other observations (for example, Laubscher, 1975, 1976).

PARALLEL KINK FOLDING BY CHANGE IN DIP OF A FAULT

Introduction.—In many practical as well as scientific problems of subsurface exploration we wish to predict the complete shape of a system of folds and faults given presently available information, prior to continued exploration. It is a common situation for the structure to involve slip on non-planar faults or folding of preexisting faults. Both these situations are geometrically closely related to the structure shown diagrammatically in figure 3, although most situations appear to be more complex because of more bends in the faults or several branches to the faults. Even the classic Pine Mountain thrust (fig. 2) is more complex than the simple step in decollement of figure 3. In order to develop more precise predictions of subsurface structure, especially in fold-and-thrust belts, it would be of great practical help to have a relationship between

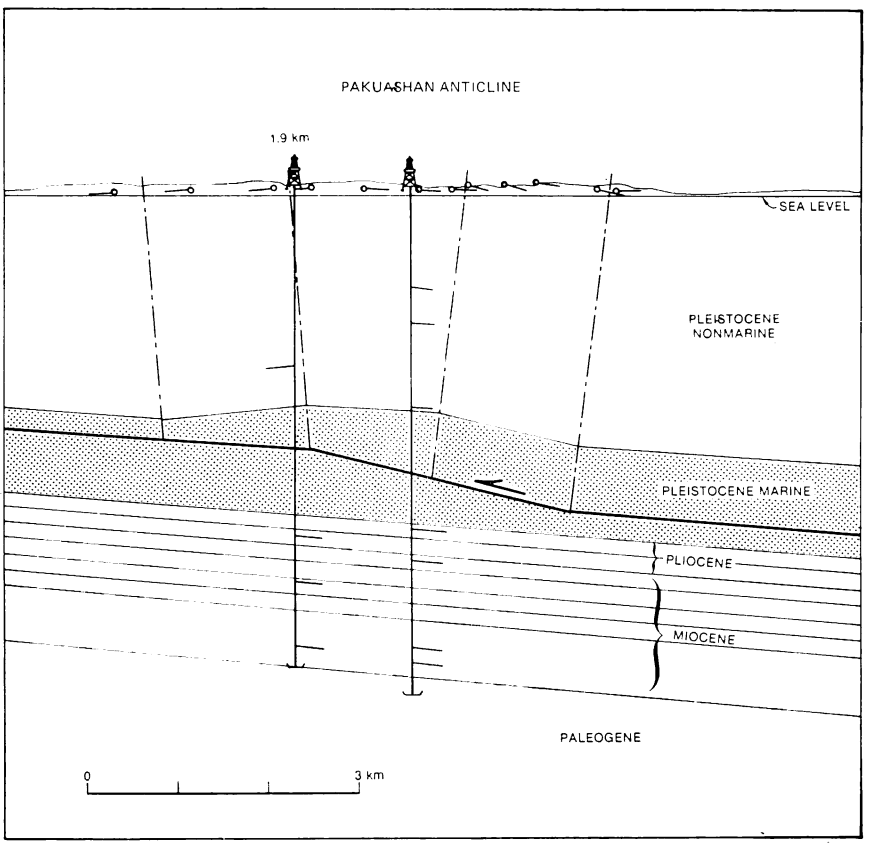

Fig. 4. Cross section of Pakuashan anticline, westcentral Taiwan, based on surface mapping, well data, and seismic data.

shapes of folds and the shapes of faults that are responsible for the folds through the mechanism of fault-bend folding.

In the following section we develop a simplified, yet widely applicable, two-dimensional geometric and kinematic theory of folding due to slip past a series of sharp bends in a fault (fig. 5). The theory is rather general. All shapes of sharp bends can be considered; curved bends can be treated as a series of sharp bends. Both convex and concave fault bends and associated anticlinal or synclinal folds can be treated. Even folding of faults, together with their adjacent beds, can be studied.

The primary geometric assumptions of the two-dimensional theory are sharp fault bends, conservation of area, and constant layer thickness normal to bedding (fig. 5), which imply conservation of bed length, deformation by layer-parallel slip, and angular kink (chevron) folds of infinite curvature and straight limbs. By these assumptions the axial surface bisects the angle between the two fold limbs ($\gamma_1 = \gamma_2$ in fig. 5); we call the angle γ the *axial angle*. Many actual fault-bend folds closely approximate these assumptions, as mentioned in the previous section, thus giving the theory some usefulness. More complex theories involving unequal axial angles or three-dimensional fault-bend folds may be developed with more effort. The next section presents the mathematical details. Applications are given in later sections.

Details of two-dimensional geometry.—We solve the geometric problem in two dimensions of what change in dip ϕ of a cross-cutting fault will produce a fold of a given axial angle ($\gamma_1 = \gamma_2$) (fig. 5). The initial angle between bedding and the fault, prior to slipping past the bend, is θ (fig. 5). It is assumed that the bedding thickness remains constant during folding, that the fold is angular, and that the deformation conserves area. It follows that the deformation is by slip parallel to bedding and that bed length is preserved during deformation. General shear within a fault-block is excluded under many circumstances by the assumptions, and for

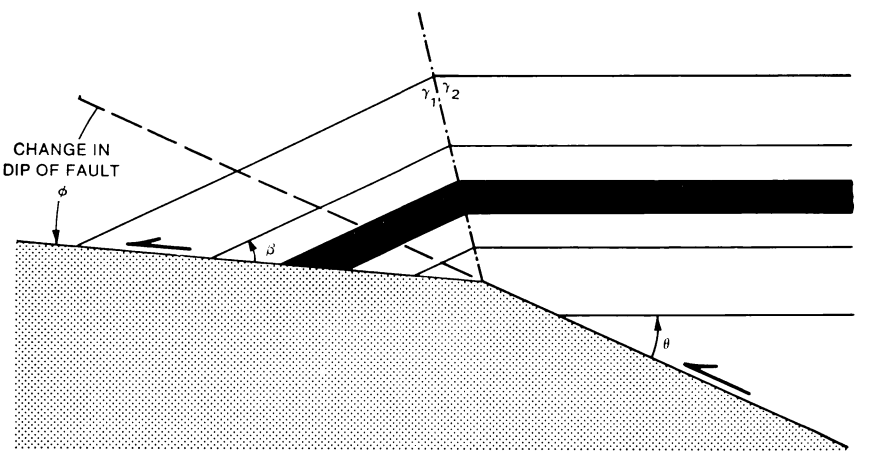

Fig. 5. Geometry of a generalized parallel-kink fault-bend fold (after Suppe, 1979).

the present we exclude all shear unrelated to riding over fault bends. Later we consider several important ancillary phenomena that involve additional layer-parallel shear.

The area of the deformed beds (triangle $a\ b\ d$ in fig. 6) must equal original undeformed area (triangle $a\ b\ c$). Similarly, deformed and undeformed bed lengths must be equal; thus lines $b\ d$ and $b\ c$ are both of length l in figure 6. Given these two constraints we can solve for the change in dip of the fault ϕ in terms of θ and γ (figs. 5 and 6).

Line segment $b\ d$ of length l is divided at point e into two segments $b\ e$ and $e\ d$ (fig. 6) where

$$b\ e = \frac{l \sin \theta}{\sin (2\gamma - \theta)} \tag{1}$$

by the law of sines. Similarly applying the law twice

$$e\ d = \frac{l \sin\gamma \sin\phi}{\sin(\phi+\gamma-\theta) \sin(2\gamma-\theta)} \tag{2}$$

Adding eqs (1) and (2) we have

$$b\ e + e\ d = l = \frac{l \sin\theta}{\sin(2\gamma-\theta)} + \frac{l \sin\gamma \sin\phi}{\sin(\phi+\gamma-\theta) \sin(2\gamma-\theta)} \tag{3}$$

Expanding this equation we get

$$1 = \frac{\sin\theta}{\sin(2\gamma-\theta)} + \frac{\sin\gamma \sin\phi}{\sin 2\gamma-\theta) [\sin\phi\cos(\gamma-\theta) + \cos\phi\sin(\gamma-\theta)]} \tag{4}$$

Multiplying by the denominator of the second term on the right and dividing by $\sin \phi$ we obtain

$$\begin{aligned} &\sin(2\gamma-\theta) [\cos(\gamma-\theta) + \cot\phi\sin(\gamma-\theta)] \\ &= [\cos(\gamma-\theta) + \cot\phi\sin(\gamma-\theta)] \sin\theta + \sin\gamma\,, \end{aligned} \tag{5}$$

rearranging we find

$$-\cot\phi = \frac{\cos(\gamma-\theta) [\sin(2\gamma-\theta) - \sin\theta] - \sin\gamma}{\sin\gamma-\theta) [\sin(2\gamma-\theta) - \sin\theta]}\,. \tag{6}$$

Finally we have

$$\phi = \tan^{-1}\left[\frac{-\sin(\gamma-\theta) [\sin(2\gamma-\theta) - \sin\theta]}{\cos(\gamma-\theta) [\sin(2\gamma-\theta) - \sin\theta] - \sin\gamma}\right] \tag{7}$$

The new angle β between the fault and bedding, after slip past the bend in the fault, is given by the equation

$$\beta = \theta - \phi + (180°-2\gamma) = \theta - \phi + \delta \tag{8}$$

where $\delta = (180°-2\gamma)$ is the change in dip across the axial surface. In some practical cases the angle β is more easily estimated than θ, ϕ, or even γ. In these cases eq (8) is a useful addition to eq (7).

We must establish certain sign conventions and ranges of angles. We define $90° \geqslant \theta \geqslant -90°$, $180° \geqslant \gamma \geqslant 0°$, $90° \geqslant \phi \geqslant -90°$, $180° \geqslant \beta \geqslant -180°$, and

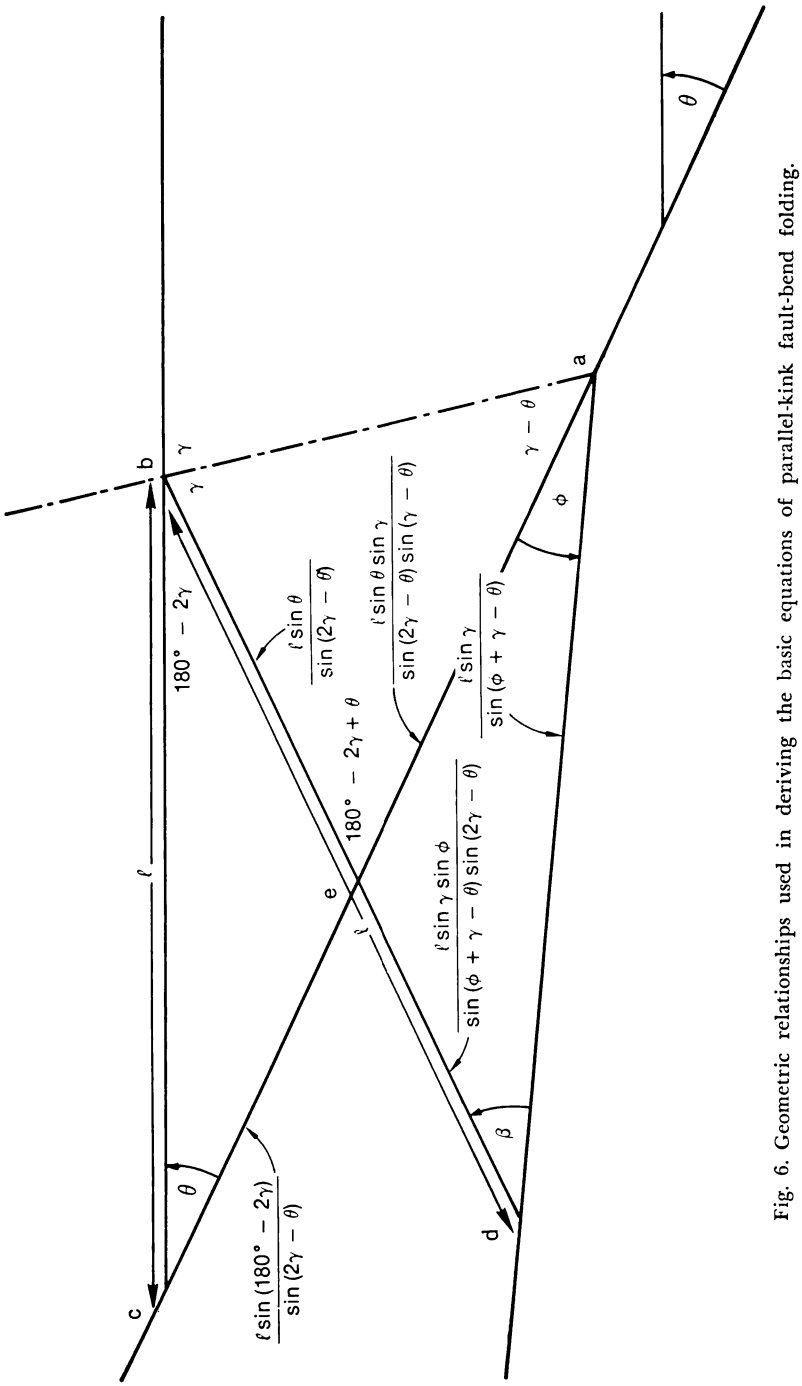

Fig. 6. Geometric relationships used in deriving the basic equations of parallel-kink fault-bend folding.

$180° \geqslant \delta \geqslant -180°$. Briefly, ϕ is measured from the projection of the first fault to the second fault and is positive for folds that are convex to the fault ("anticlines"). β and θ are positive in the same direction — clockwise or anticlockwise — as ϕ and are both measured from the fault to the same side of the bed (note $|\theta| \leqslant 90°$). δ is the same sign as ϕ if its direction is the same as ϕ (positive for anticlines). δ is measured from the projection of the bed in the same direction as θ.

The above sign conventions are unduly complex for most practical problems not involving slip over multiple positive and negative fault bends (+ and − ϕ). The problem is simplified if we consider all folds convex toward the fault as "synclines" and all folds concave toward the fault as "anticlines"; we define $90° \geqslant \gamma \geqslant 0°$, $90° \geqslant \phi \geqslant 0°$, $90° \geqslant \theta \geqslant -90°$, $180° \geqslant \beta \geqslant -90°$, and $180° \geqslant \delta \geqslant 0°$. β and θ are measured from the fault to the same side of the bed (note $|\theta| \leqslant 90°$) and are positive for "anticlines" and negative for "synclines". Figure 7 presents graphs of eqs (7) and (8), using the simplified sign conventions. "Anticlines" are to the left, and "synclines" are to the right.

Equation of a simple step in decollement.—Folds that involve a simple step from one decollement to another (fig. 3) are sufficiently important that it is useful to derive the fault-bend folding relationship (eq 7) for this special case, namely

$$\phi = \theta \tag{9}$$

Combining with eq 4 we obtain

$$\sin(2\gamma - \theta) = \sin\theta + \frac{\sin\gamma\sin\theta}{[\sin\theta\cos(\gamma - \theta) + \cos\theta\sin(\gamma - \theta)]} \tag{10}$$

Simplifying using trigonometric identities we obtain

$$\tan\theta = \frac{\sin 2\gamma}{2\cos^2\gamma + 1} \tag{11}$$

and

$$\phi = \theta = \tan^{-1}\left[\frac{\sin 2\gamma}{1 + 2\cos^2\gamma}\right] \tag{12}$$

which is the relationship between cutoff angle θ or fault bend ϕ and fold shape γ for a simple step in decollement. A graph of eq (12) is given as part of figure 7.

Discussion of the fault-bend folding equations.—The above equations, especially 7, 8, and 12, have many practical applications in attempts to predict the subsurface geometry of structures. The assumptions are two dimensions, conservation of area and bed length, and no general affine shear. These imply slip parallel to bedding. If a structure cannot be successfully described by these equations then either it is not a fault-bend fold, the assumptions are not valid, or the structure is too complicated to solve given the limited data available. Thus the equations are useful whether or not the structure is actually of the parallel-kink fault-bend mechanism, because they are a standard against which the structure can be quantitatively compared.

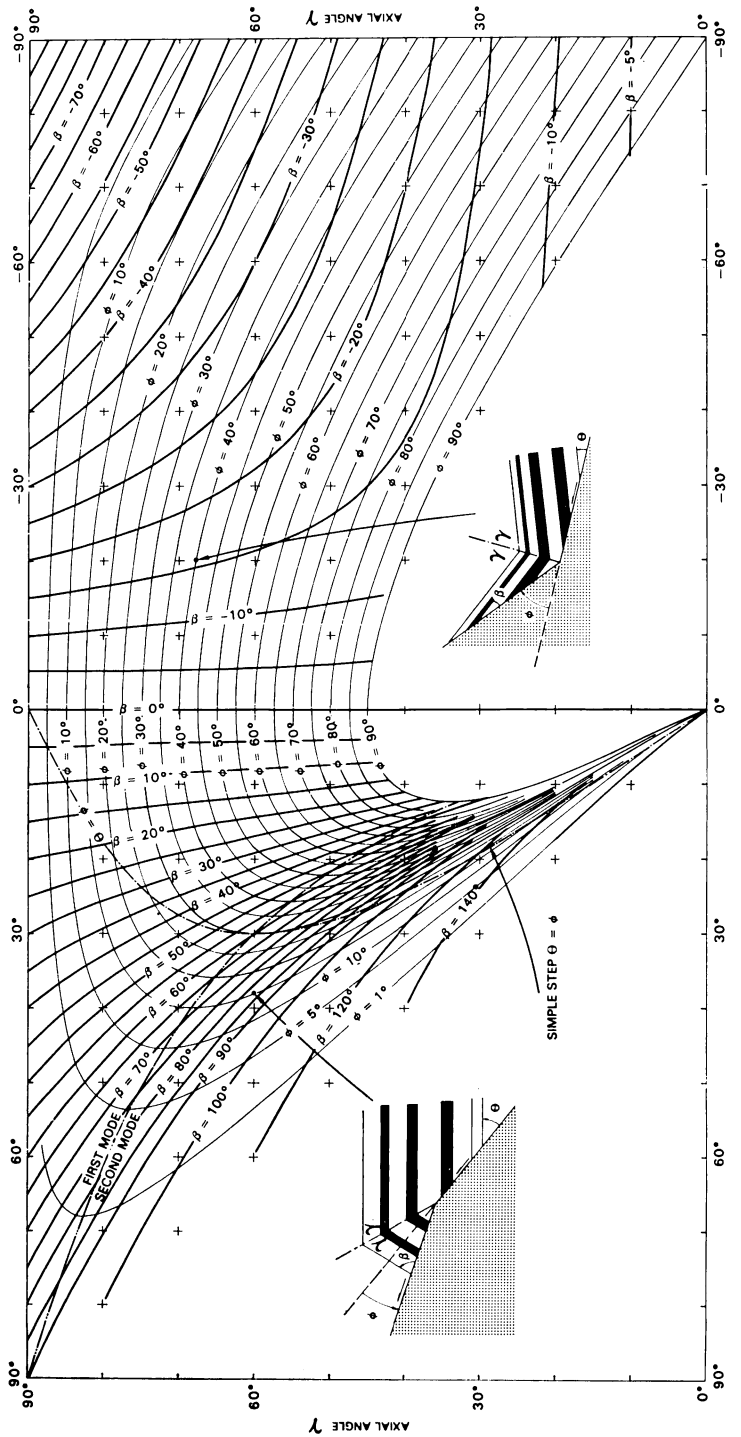

Fig. 7. Graph of relationships between fold shape γ, fault shape ϕ, and cutoff angles θ and β for parallel-kink fault-bend folding; based on eqs 7, 8, and 12.

A graph of eqs (7), (8), and (12) has been prepared (fig. 7) to allow quick visual analysis of the possible range of solutions to a given problem. For example, if an anticline has an observed axial angle γ of 83° then an associated change in fault dip ϕ cannot be greater than about 16° to 17°; furthermore ϕ of less than 10° is not possible for a large range of θ and β. If the bend is a simple step, then the cutoff angle $\theta = \phi$ is 14°. Thus the range of possible solutions can be quickly assessed. For this reason it is more efficient in most practical applications to use the graph than to use the equations directly.

The graph in figure 7 plots θ against γ showing lines of constant ϕ and β. A notable feature of the graph is that γ is a double-valued function of θ and ϕ for "anticlines"; thus, for a given fault bend ϕ and initial cutoff angle θ there are two possible shapes in the fold γ. For example, if $\theta = \phi = 20°$, then the axial angle γ can be 78° or 32°; the larger values of γ are called *first-mode folds*, and the smaller values are called *second-mode folds* (fig. 8). The boundary between the two modes on the graph is

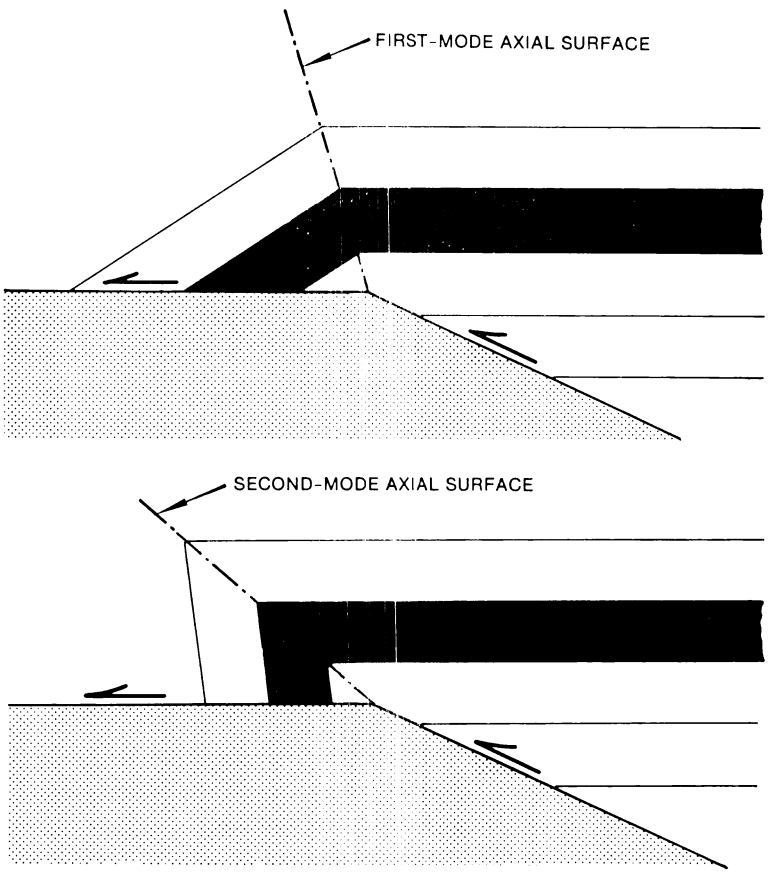

Fig. 8. The two modes of fault-bend folding for $\theta = \phi = 25°$ (after Suppe and Namson, 1979).

marked with a dashed line (fig. 7). It may be questioned whether or not both geometrically possible modes are mechanically possible; for example, the first mode might be favored by its smaller bending and bedding-plane slip. Nevertheless, there is some indication that second-mode folds might form; for example, Suppe and Namson (1979) present some subsurface interpretations involving second-mode simple-step folding. It is important to be cautious in interpreting folds with steep to overturned front limbs as second-mode fault-bend folds, because fault-propagation folds have a shape that is difficult to distinguish in the subsurface from second-mode fault-bend folds, as will be discussed elsewhere. Our present experience is that most fault-bend fold structures are first-mode folds or complex imbricated stacks of first-mode folds.

A second important aspect of the graph (fig. 7) is that for a given initial cutoff angle θ there exists a maximum angle of fault bend ϕ for which layer thickness is preserved in anticlinal folds because of the double-valued nature of eqs (7) and (12). For example in the case of a simple ramp in decollement the maximum angle of stepup ($\phi=\theta$) is 30° without thinning of beds (non-parallel folding). As another example, a reverse fault stepping up at 55° to bedding cannot flatten more than 4° without experiencing local layer thinning or secondary faulting. Therefore, information on layer thickness around suspected fault-bend folds offers a potential constraint on possible fault bends at depth. The range of possible fault bends for which layer thickness is preserved is even more restricted in cases of multiple imbrications, as is discussed later in this report.

Simple application of fault-bend fold equations.—The most straightforward applications of the fault-bend fold equations are in the solution of well-constrained problems or parts of problems involving simple bends in faults. For example, the fold shape (γ) (fig. 5) may be well known, and we may wish to compute the shape of a fault (ϕ) capable of producing the fold, given the orientation of the fault (θ or β) in one part of the structure. An actual example is given in the following paragraphs. The equations also may be used to solve more complex problems of imbricate structures as is explained near the end of this report.

Figure 9 presents as an example an incomplete cross section of the crest of the Hukou-Yangmei anticline in the fold-and-thrust belt of western Taiwan. The cross section is constrained by detailed surface mapping, two wells, and some seismic data. Well A is unusual because it encountered a double thickness of the distinctive Pliocene Chinshui Shale and normal thicknesses of formations below the Chinshui Shale, suggesting that the small fold on which well A sits does not extend below the Chinshui Shale. Let us make the hypothesis that the fold is a fault-bend fold associated with a fault that repeats the Chinshui Shale in well A; we now attempt to test this hypothesis.

This example from Taiwan is typical of simple applications of the fault-bend fold equations; we have a general structural hypothesis, and we wish to test it quantitatively. In order to do this we must guess a specific solution. Two guesses are shown in figure 10, both involving the

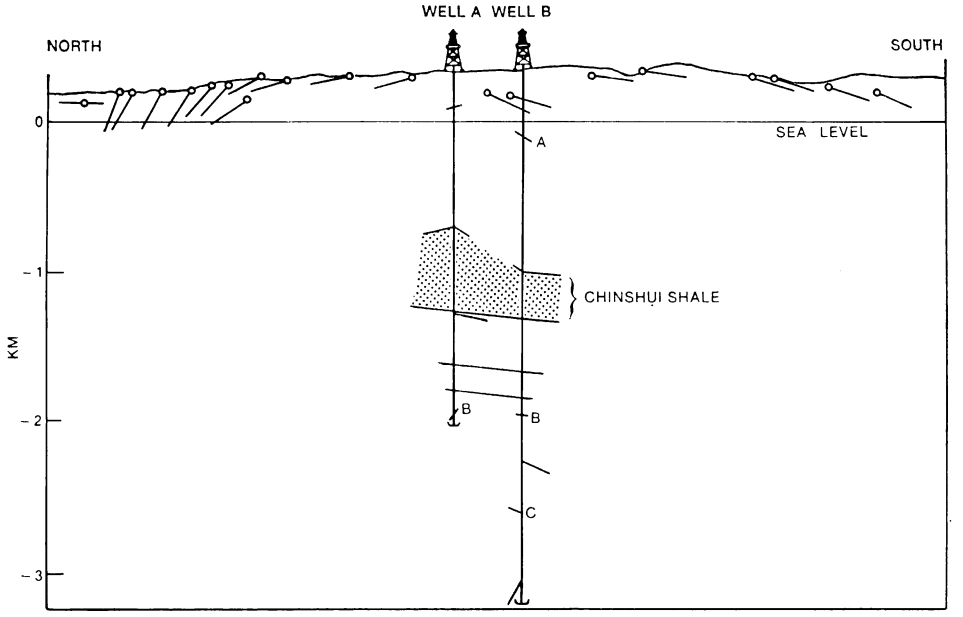

Fig. 9. Basic surface and subsurface data, Hukou-Yangmei anticline, northern Taiwan.

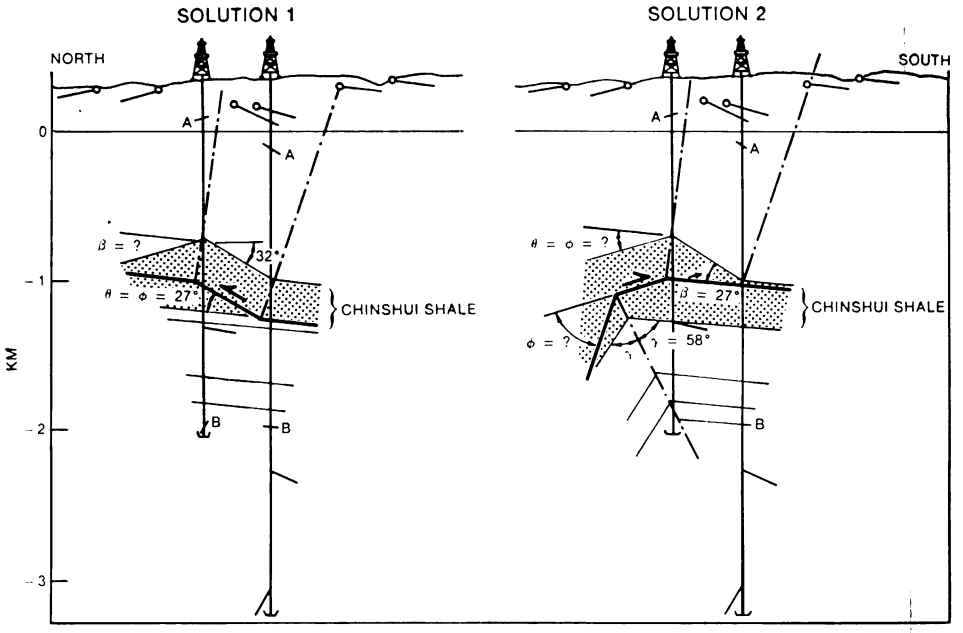

Fig. 10. Two potential solutions for the thickening of Chinshui Shale by fault-bend folding, Hukou-Yangmei anticline, northern Taiwan.

simple step of a thrust from one decollement to another in the Chinshui Shale. In solution 1 a thrust steps up to the north, whereas in solution 2 a thrust steps up to the south. The critical angular observations are that the dip at the base of the Chinshui Shale and below is 5°, whereas the minimum dip of the top of the Chinshui Shale, between the two wells, is 32° with similar but slightly lower dips observed at the surface off the line of section. Therefore we choose 32°–5° = 27° as $\theta = \phi$ in solution 1 and β in solution 2. Using figure 7 we determine $\beta = 34°$ for solution 1 with 34°–5° = 29° as the predicted surface dip. This surface dip is substantially greater than the observed surface dip of about 16° so we discard solution 1 as incorrect. Using figure 7 we determine $\phi = \theta = 22°$ for solution 2 and 22°—5° = 17° as the predicted surface dip, in good agreement with observation. We therefore consider solution 2 viable.

Further fault-bend computations are possible in this example. An anticline is present at depth, as shown by these and other wells. We now compute how the shallow fault in solution 2 will be folded by the deeper anticline ($\gamma = 58°$). The crosscutting fault block is on the footwall, convex toward the fault; therefore it corresponds to a "synclinal" geometry in figure 7, as may be seen by viewing figure 10 upside down. We observe $\theta = -22°$ and $\gamma = 58°$ for a "synclinal" geometry; therefore we determine from figure 7 that $\phi = 57°$ and $\beta = 15°$, which are in reasonable agreement with surface dips. A final version of the Hukou-Yangmei cross section (fig. 11), incorporates solution 2.

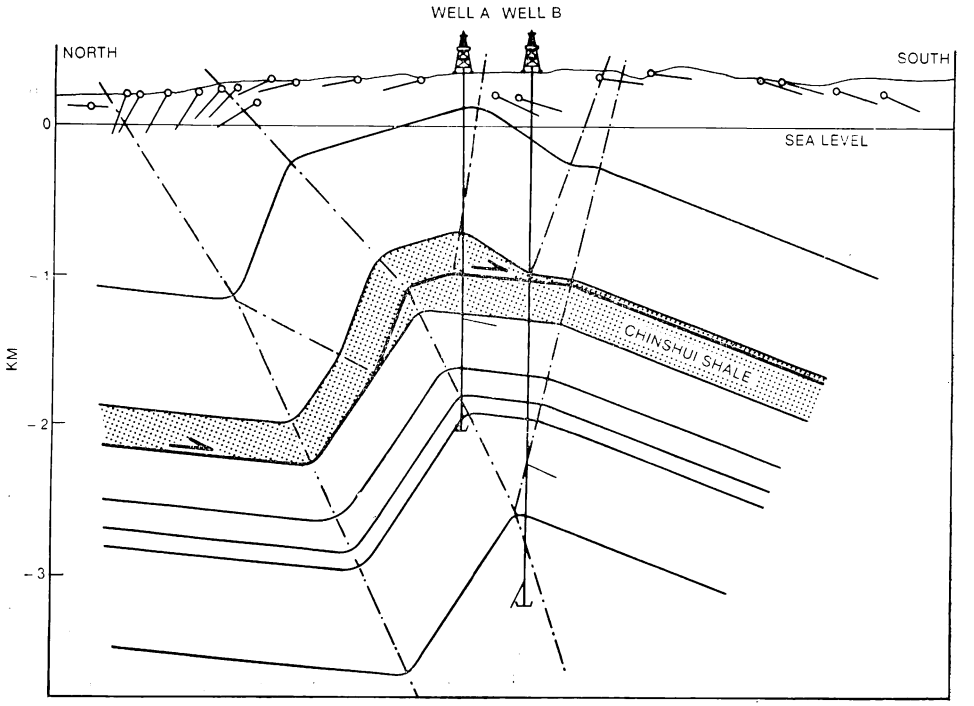

Fig. 11. Completed fault-bend folding interpretation of the shallow part of Hukou-Yangmei anticline, based on solution 2, figure 10.

ADDITIONAL ASPECTS OF PARALLEL-KINK FAULT-BEND FOLDS

In the present section we treat additional aspects of the geometric and kinematic description of parallel-kink fault-bend folds. These include (1) change in fault slip across a fault-bend fold, (2) multiple bends in a single fault, (3) shearing of fault-bend folds by layer-parallel slip in the thrust sheet, and (4) the branching of axial surfaces within the folded sheet. One further aspect, which is so important that it is treated in a separate section, is the geometric description of parallel-kink fault-bend folds involving multiple fault imbrications. This topic is discussed in the final section of this report, "Imbricate Fault-Bend Folding."

Change in fault slip across a fault-bend fold.—Fault slip is not conserved across a fault-bend fold if the fault cuts across bedding in the folded sheet. The slip may increase or decrease as a result of folding, although decreases are quantitatively more important. Continuing with the same assumptions as above, if $a\ c$ is the fault slip before the bend and $a\ d$ is the fault slip beyond the bend (fig. 6), then we may define a *ratio of slips* R as

$$R = \frac{a\ d}{a\ c} = \frac{\text{slip beyond bend}}{\text{slip before bend}} \tag{13}$$

By the law of sines we have

$$a\ c = \frac{l \sin (180°-\gamma)}{\sin (\gamma-\theta)} = \frac{l \sin \gamma}{\sin (\gamma-\theta)} \tag{14}$$

also

$$a\ d = \frac{l \sin \gamma}{\sin (\phi+\gamma-\theta)} \tag{15}$$

Combining (13), (14), and (15) we obtain an expression for the slip ratio

$$R = \frac{\sin (\gamma-\theta)}{\sin (\phi+\gamma-\theta)} \tag{16}$$

A graph of the ratio of slips R (eq 16) is given in figure 12. We first note that if the fault is not cross cutting ($\theta = 0°$), fault slip is preserved across the fault bend. If the fault is cross cutting ($\theta \neq 0°$) slip is increased in synclinal folding ($R > 1$) and decreased in anticlinal folding ($R < 1$). Note in figure 12 that decreases in slip are generally more substantial than increases in slip. Increases in slip are generally on the order of 10 to 20 percent or less ($R = 1.1$ to 1.2) for typical synclinal fault-bend folds, whereas decreases may reach 40 percent ($R = 0.6$) for first-mode simple-step anticlines and 60 percent ($R = 0.4$) for many second-mode simple-step anticlines. Therefore slip is not preserved across fault bends in thrust sheets that cross cut bedding. Fault slip is consumed or produced by folding within the thrust sheets.

Theory of multiple fault bends.—Many faults, especially thrust faults, have sufficiently large slip that the beds may have slipped past more than one bend in the fault. We now consider what effect the sequence of fault bends has on the final shape of the beds (γ, β). If the sequence of fault

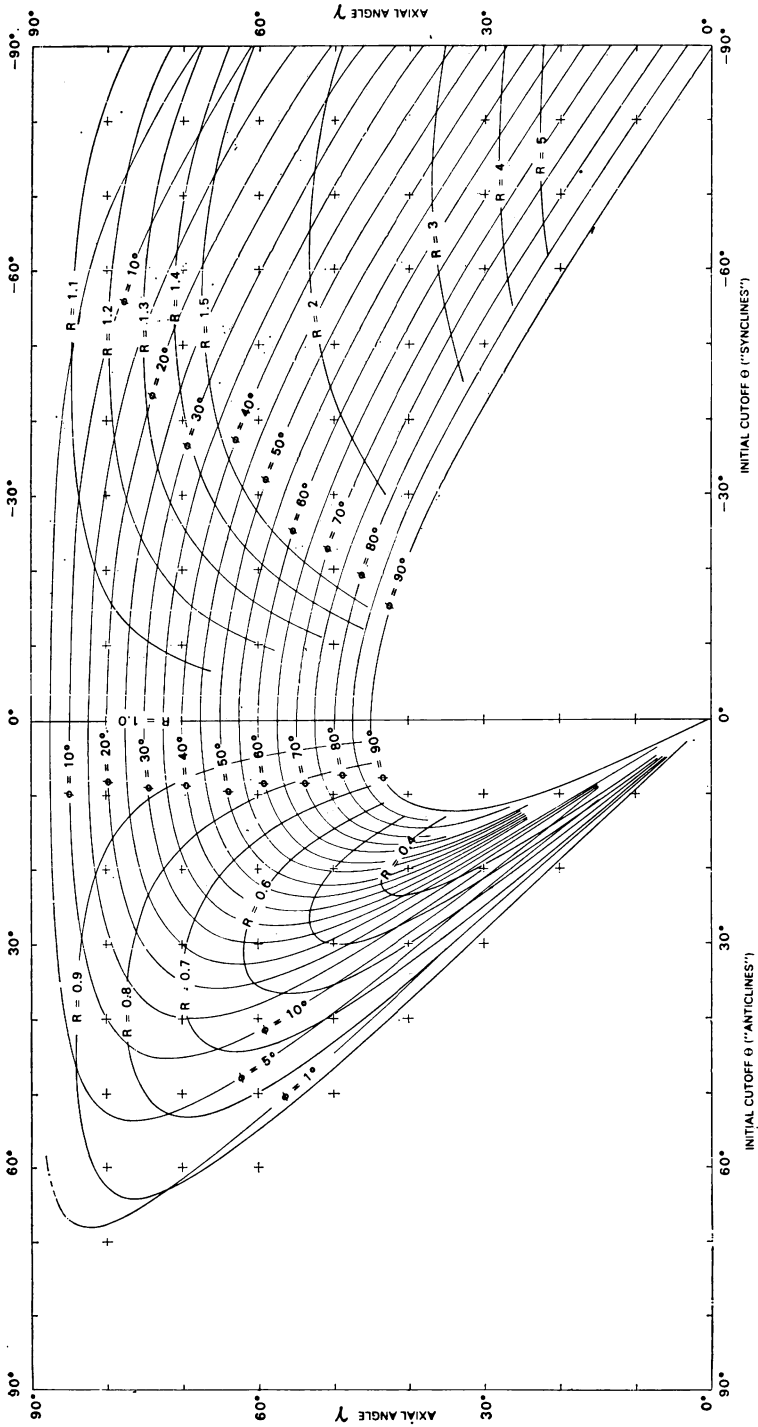

Fig. 12. Ratios of slips R across fault-bend folds, based on eq 16. "Anticlines" consume slip ($R<1$) and "synclines" produce slip ($R>1$).

bends is labeled ϕ_1, ϕ_2 . . . ϕ_n then the *net bend* in the fault Φ between $i = 1$, and $i = n$ is

$$\Phi = \sum_{i=1}^{n} \phi_i . \tag{17}$$

For a sequence of bends, β_n of a previous bend is θ_{n+1} for the next bend (fig. 13); therefore from eqs (8) and (17) we have

$$\beta_1 = \theta_1 - \phi_1 + (180° - 2\gamma_1) = \theta_2$$
$$\beta_2 = [\theta_1 - \phi_1 + (180° - 2\gamma_1)] - \phi_2 + (180° - 2\gamma_2) ,$$

and

$$\beta_n = \theta_1 - \Phi + \sum_{i=1}^{n} (180° - 2\gamma_n) \tag{18}$$

The change in dip of the beds across the i-th fold γ_i is

$$\delta_i = (180° - 2\gamma_i) . \tag{19}$$

Thus the *net change in dip* Δ is the last term of eq (18)

$$\Delta = \sum_{i=1}^{n} (180° - 2\gamma_i) = \sum_{i=1}^{n} \delta_i , \tag{20}$$

and eq (18) becomes

$$\beta_n = \theta_1 - \Phi + \Delta . \tag{21}$$

The net change in dip of beds, Δ, is obviously a function of the sequence of fault bends because it depends on the choice of mode of folding ($k = 1$ or 2) at each fault bend. Furthermore, even if we confine ourselves to a single mode, for example first mode, the final cutoff angle β_n and the net change in dip Δ both depend on the sequence of fault bends because they are not linearly related to θ and ϕ (eqs 7 and 8):

$$\beta_n (\phi_i, k_i) \qquad i = 1 \rightarrow n, k_i = 1 \text{ or } 2$$
$$\Delta (\phi_i, k_i) \qquad i = 1 \rightarrow n, k_i = 1 \text{ or } 2$$

The dependence of final cutoff angle on the sequence of fault bends is illustrated with two examples in figure 13, which also illustrate the effects of convex and concave ramps along thrust faults. In example 1 a net fault bend $\Phi = 30°$ with an initial cutoff of 30° is accomplished in one case (1A) with a single 30° bend ($\Phi = \phi_1 = \theta_1 = 30°$) producing a final cutoff $\beta = \Delta = 60°$, whereas in the other case (1B) the same net bend is accomplished by a series of three 10° bends ($\phi_1 = \phi_2 = \phi_3 = 10°$) producing a different final cutoff $\beta_3 = \Delta = 49°$. In example 2 a net fault bend $\Phi = 15°$ with an initial cutoff of 15° is accomplished in one case (2A) with a single 15° anticlinal bend ($\Phi = \phi_1 = \theta_1 = 15°$) producing a final cutoff $\beta = \Delta = 16°$, whereas in the other case (2B) the 15° net bend

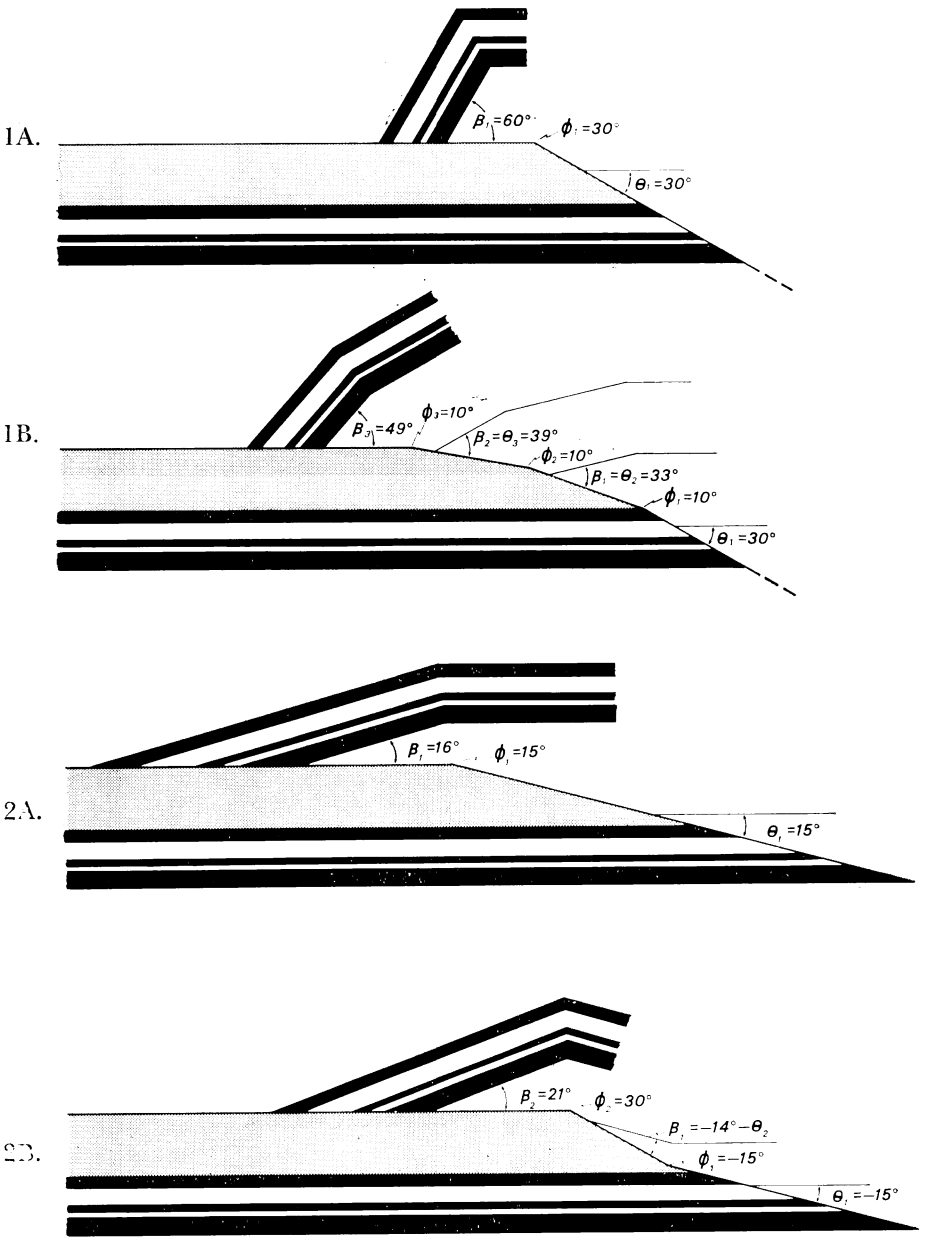

Fig. 13. Two illustrations of the dependence of final cutoff angle β_n on the sequence of fault bends (ϕ_1, ϕ_2, . . . ϕ_n) given the same net fault bend Φ and initial cutoff angle θ_1.

is accomplished by first a synclinal bend $\phi_1 = -15°$ and then an anticlinal bend $\phi_2 = +30°$ producing a final cutoff $\beta_2 = 21°$. These examples have no associated scale. In actual structures the fault-bend folds typically do not propagate a long distance into the overlying fault block if the distance between the bends is very small relative to the thickness of the fault block, instead the folds are dissipated in disharmonic, non-parallel behavior.

It should be noted that if we can measure the final cutoff angle β_n and the net change in dip Δ, which may be possible in practical problems, we can calculate $(\theta_1 - \Phi)$ using eq (21)

$$\beta_n (\phi_i, k_i) = \theta_1 - \Phi + \Delta(\phi_i, k_i) \tag{22}$$

because initial cutoff angle θ_1 and net fault bend Φ are independent of the sequence of bends or mode numbers.

Shearing of fault-bend folds.—Our theoretical development of the previous sections included the important constraint that the beds only undergo shear as they pass through a fault-bend fold; in particular the beds on the right side of the fold in figure 5 undergo no shear until they pass through the axial surface. We now relax this constraint to consider two important ways in which zones of layer-parallel shear within a thrust sheet or other fault block can deform parallel fault-bend folds: (1) shearing-out of flat fold crests and (2) general layer-parallel shear in parallel fault-bend folding.

1. *Shearing out of flat fold crests*: The ideal theoretical shape of a simple-step fold is shown in figure 3; however Suppe and Namson (1979) pointed out that several folds of western Taiwan exhibit an important deviation from this ideal shape. These modified structures exhibit a squeezing out of the flat crest of the ideal structure, as is shown in figure 14.

The squeezing out of the flat crest of the anticline is accomplished by simple shear within the thrust sheet. This shear is possible within the confines of the present theory when the line of the hanging-wall cutoff Y' is in contact with the line of the footwall cutoff X (figs. 3 and 14). Only at this stage in the deformation are axial surfaces A and B' in contact along X-Y' and able progressively to annihilate each other to form a new axial surface $(AB')^*$ by the mechanism shown in figure 14. The annihilation involves locking of the primary fault surface and slip in turn along progressively higher bedding surfaces, resulting in a layer-parallel shear of the thrust sheet above the lower decollement in the hanging wall. The active slip surface is always the bed in contact with the branch in axial surface (fig. 14). All slip is absorbed in the annihilation, therefore the thrust sheet is immobile along the upper decollement, beyond the anticlinal axial surface $(AB')^*$.

Applying the geometry of annihilation of the flat crest of a simple-step fold as shown in figure 15A we obtain an expression for the shortening or displacement d associated with annihilation along any given bed

$$d = c + b - a \tag{23}$$

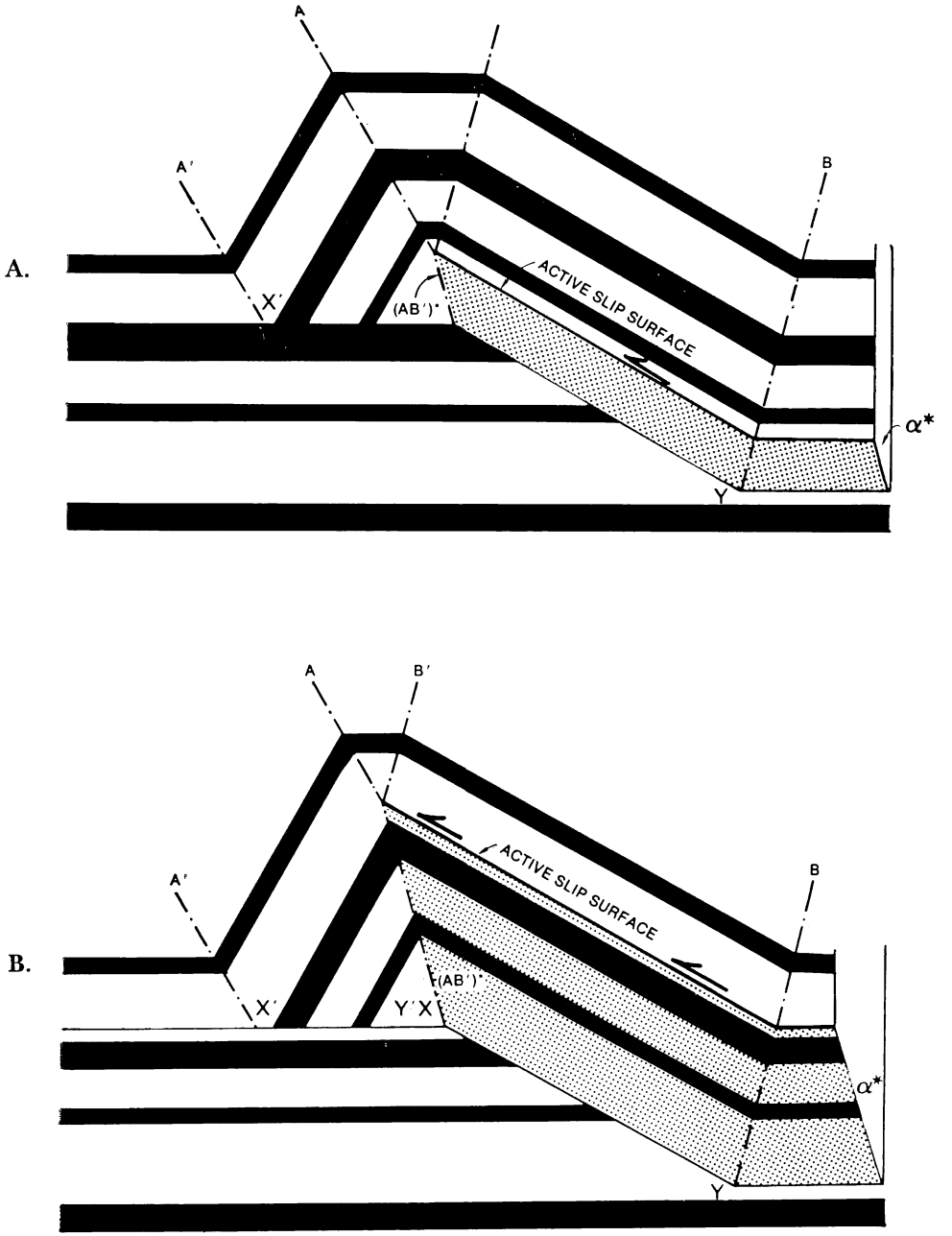

Fig. 14. Kinematics of annihilation of a flat fold crest.

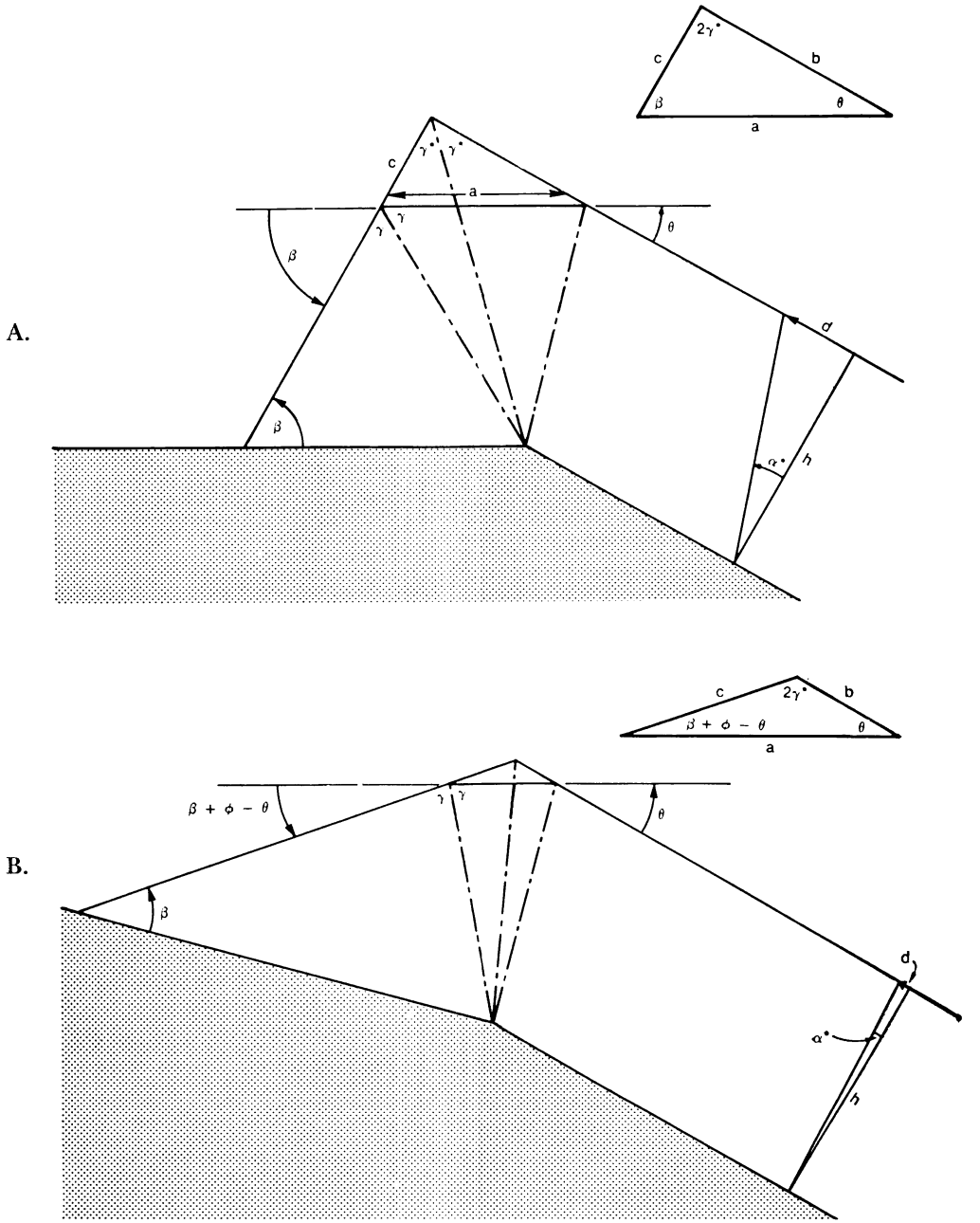

Fig. 15. Geometric elements for computing the shear associated with squeezing out of flat fold crests.

Applying the law of sines we obtain

$$d = a\left[\frac{\sin\beta + \sin\theta}{\sin 2\gamma^*} - 1\right] \tag{24}$$

where $\gamma^* = (180° - \beta - \phi)/2$ is the axial angle of the new axial surface $(AB')^*$. The width a of the annihilated flat top of the anticline is a function of stratigraphic height h above the lower decollement

$$a = h\,[\cot\gamma + \cot(90° - \theta/2)] \tag{25}$$

Combining eqs (24) and (25) we obtain the expression for the simple shear $S^* = d/h$ associated with the annihilation of the flat top of a simple-step fold (figs. 14 and 15A).

$$S^* = d/h = [\cot\gamma + \cot(90° - \theta/2)]\left[\frac{\sin\beta + \sin\theta}{\sin 2\gamma^*} - 1\right] \tag{26}$$

A more general form of the equation, not confined to simple-step folds (fig. 15B), is

$$S^* = d/h = [\cot\gamma + \cot(90° - \theta/2)]\left[\frac{\sin(\beta+\phi-\theta) + \sin\theta}{\sin 2\gamma^*} - 1\right] \tag{27}$$

The angular shear α^* is

$$\alpha^* = \cot^{-1}S^* \tag{28}$$

The angular shear α^* for all simple-step folds is shown in figure 16. For first-mode simple steps of less than 20° ($\phi = \theta$) the shear is negligible (less than 2°). The shear increases to 17.2° for a step of 30° $= \phi = \theta$ and becomes progressively larger for second mode folds of smaller axial angle γ. Therefore substantial distortion of the hangingwall sheet is associated with annihilation. The distortion of faults farther back in the hanging wall sheet is, however, less severe because the faults will generally be at an angle to bedding of less than 30°. The dip of faults of the same angle ($\theta = \phi$) as the simple step is subject to a maximum flattening of 6.94° at $\theta = \phi = 23.5°$ (second mode). The flattening of faults in the hanging-wall sheet is less than 2° for most first-mode folds ($\theta = \phi \leqslant 27°$) and therefore needs only be considered in second-mode simple-step folding.

The shearing of a simple-step fault-bend fold with associated annihilation of axial surfaces, as shown in figure 24, is not inevitable. For example, the Pine Mountain thrust sheet (fig. 2) has not undergone this shear. Nevertheless, the shearing appears to be a widespread process (for example, Suppe, 1980b; Suppe and Namson, 1979), particularly in multiple imbrication structures (fig. 24), and may be a mechanism by which thrust sheets become locked. The shallow thrust in figure 11 is in locked position, for example. We recall that during annihilation, the primary fault is locked (fig. 14). If the stresses are high enough to release the fault, then the structure will be released from its associated ramp; at present we know no natural structures of this type. Apparently their formation is inhibited by resistance to the bending associated with axial surfaces that

must form during their release. The propagation of a new fault or imbrication may require a lower stress. Locked thrust sheets with annihilated axial surfaces similar to figures 11 and 14 appear to be widespread.

2. *General layer-parallel shear in parallel fault-bend folding*: If we relax the constraint of no layer-parallel shear of the beds prior to passing through an axial surface, then a variety of new fold shapes is possible, of the sort shown in figure 17.

The old constraint of no layer-parallel shear was expressed as the requirement

$$b\,c = b\,d \tag{29}$$

in figure 6. We now allow layer-parallel shear of the sort shown in figure 17. The requirements for parallel folding then become $\gamma_1 = \gamma_2$ and

$$b\,c = b\,d + a\,b \sin\gamma \tan\alpha \tag{30}$$

where α is the angle of simple shear (fig. 17). The fault-bend fold equations may now be rederived including the last term in eq (30). In particular eq (7) becomes

$$\phi = \tan^{-1}\left[\frac{[\sin\theta \sin\gamma \tan\alpha - \sin(\gamma-\theta)]\,[\sin(2\gamma-\theta) - \sin\theta]}{\cos(\gamma-\theta)\,[\sin(2\gamma-\theta) - \sin\theta] - \sin\gamma}\right] \tag{31}$$

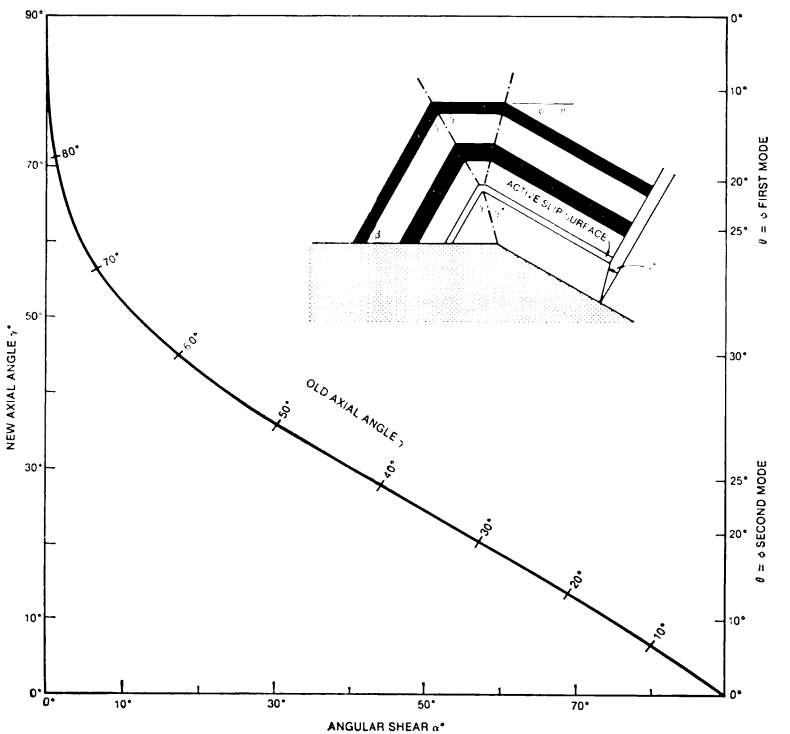

Fig. 16. Angular shear for squeezing out of flat fold crests in simple-step folds.

Eq (31) admits a wide variety of fold shapes that were impossible under the previous constraint of not allowing an arbitrary imposed shear α (fig. 17). Nevertheless our experience with actual structures whose shapes are well documented suggests that the imposed shear α is generally zero, but we know some exceptions to be discussed elsewhere. They involve reactivation of preexisting normal faults in thrust motion similar to the geometry of figure 17. Therefore they represent an exception to the rule that the highest cutoff angle $\theta = \phi$ for a simple-step parallel fault-bend fold is 30°.

Shear associated with branching axial surfaces.—Branching of axial surfaces is a widespread phenomenon in fold-and-thrust belts because of locking and shearing of thrust sheets as discussed above and because of interference of kink bands of nearby fault-bend folds. We have seen that branching of an axial surface is associated with a change in layer-parallel simple shear, as shown in figures 14 and 15. This property may be useful in predicting subsurface geology, because, in passing through a series of anticlines and synclines, shear may be conserved in a way somewhat analogous to conservation of bed length. If so, then branching in the anticlines, which is easily observed, must be balanced by equivalent branches of opposite effect in the synclines. The important point to note is that the opposite branches must occur at the same stratigraphic horizon in order to conserve layer-parallel shear. The elements of the theory are outlined below.

Any change in dip causes a shearing of the beds. If the unsheared state is horizontal, then the layer-parallel simple shear S is a simple function of dip angle δ. The geometry of the problem is shown in figure 18. By the Law of Sines

$$\frac{a}{\sin(\alpha-\delta/2)} = \frac{[a/\sin(\delta/2)]}{\sin(90-\alpha)}$$

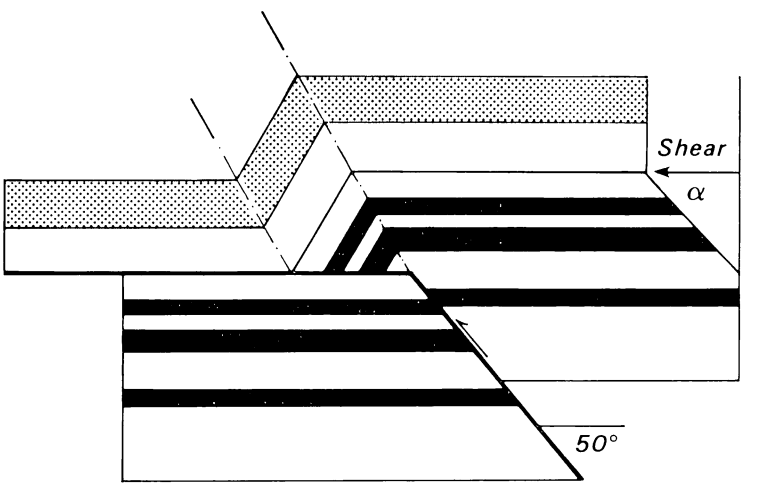

Fig. 17. An example of general layer-parallel simple shear in combination with fault-bend folding.

Rearranging we get

$$S = \tan \alpha = 2 \tan \delta/2 \tag{32}$$

Thus, by knowing the dip we may immediately compute the shear.

Eq (32) is also the expression for the shear (change in shear) associated with the change in dip across an axial surface. We can add the shears associated with axial surfaces $i = 1, 2, \ldots n$ along a single layer

$$\sum_{i=1}^{n} S_i = S_1 + S_2 + \ldots S_n = 2[\tan \delta_1/2 + \tan \delta_2/2 + \ldots \tan \delta_n/2] \tag{33}$$

There is a change in shear across a node (fig. 19) associated with the merging or splitting of axial surfaces

$$\Delta S_{12} = S_1 + S_2 - S_{12} = 2[\tan \delta_1/2 + \tan \delta_2/2 - \tan \delta_{12}/2] \tag{34}$$

ΣS can be defined for any layer and is constant for any stratigraphic interval that contains no nodes. From eqs (33) and (34) we then have for stratigraphic intervals X, Y, and Z

$$\Sigma S_x = \Sigma S_y + \Sigma \Delta S_{xy} = \Sigma S_z + \Sigma \Delta S_{xyz} \tag{35}$$

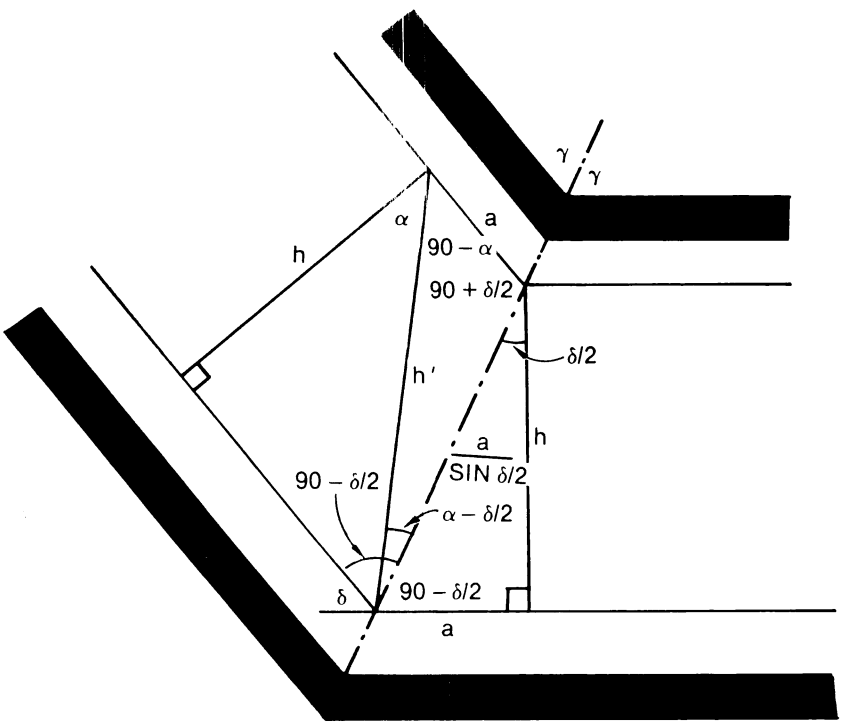

Fig. 18. Geometric elements used to determine the angular layer-parallel simple shear α associated with a change in dip δ (eq 32).

Therefore we can say that between pinning points of no shear or constant shear, the sum of the changes in shear along any bed containing nodes (nodel surface) is zero

$$\Sigma \Delta S = 0 \tag{36}$$

This fact reduces the problem of balancing a cross section across a "blind" syncline to the problem of balancing changes in shear along each nodal surface. The nodal surfaces can be discovered in the anticlines, and the amount of shear measured from the dips (eq 34). Changes in shear of the same magnitude but opposite sign must exist along the same bed in the intervening synclines.

IMBRICATE FAULT-BEND FOLDING

General experience in fold-and-thrust belts suggests that most fault-bend fold structures involve multiple imbrications. Even the type example of the Pine Mountain thrust sheet involves two imbrications (fig. 2). Therefore any useful geometric theory of fault-bend folding must be capable of dealing with imbrications in a straightforward fashion. In this section we consider imbricate fault-bend folding in which all imbrications are of the same vergence.

In general, to solve for an imbricated fault-bend fold structure such as figure 2, we need to know, or be able to compute, the undeformed cut-

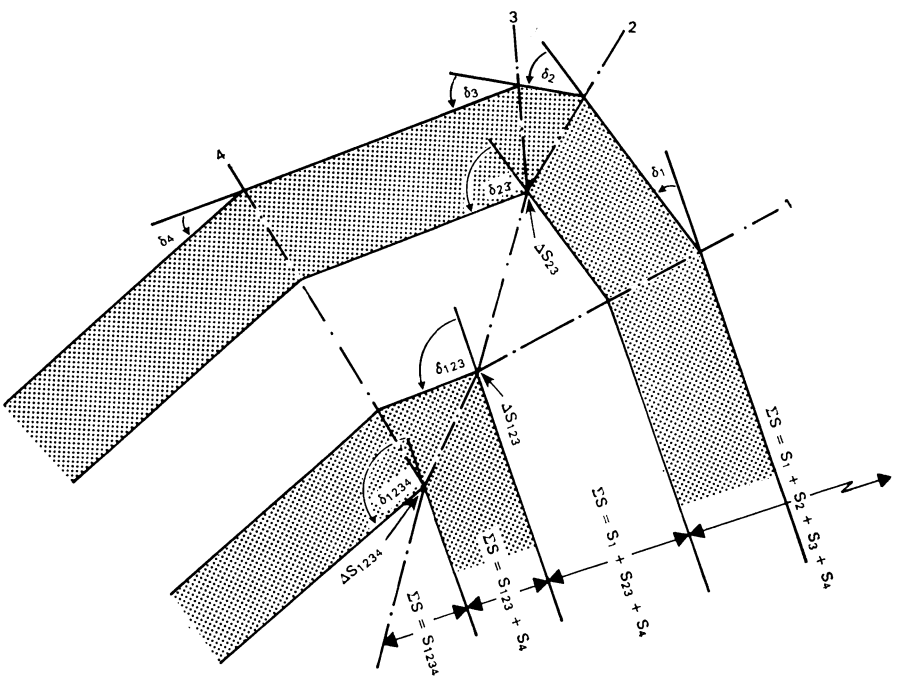

Fig. 19. Notation for changes in layer-parallel simple shear associated with branching axial surfaces. The change in shear ΔS associated with a branch is the difference in sums of shears, for example $\Delta S_{23} = (S_2 + S_3 - S_{23})$.

off angles $\phi_i = \theta_i$ for each of the imbrications. During deformation, these cutoff angles may change because of shear associated with folding of the thrust sheets and annihilation of axial surfaces. Nevertheless, if we know the undeformed cutoff angles, here called the *fundamental-cutoff angles*, $^{\circ}\theta_1$, $^{\circ}\theta_2$, . . . $^{\circ}\theta_n$, we can solve all the angular relations of an imbricate structure as outlined below.

With each successive imbrication there is a quantum increase in forward and back dip. Therefore within an imbricate fault-bend fold, panels of rock bounded by axial surfaces may be classified according to the number of underlying imbrications (fig. 20). We will label the number of imbrications associated with a panel of rock using numerals 0, I, II, III . . . , with 0 indicating a panel of regional dip. To calculate quantum jumps in back dip and forward dip associated with successive imbrications we derive trigonometric relationships between the cutoff angles of imbrications ($^{\circ}\theta_n$) and the dips of rock panels in the fault-bend folds.

Back dips associated with imbrication.—An imbrication of fundamental-cutoff angle $^{\circ}\theta_1 = \delta$ produces a shear S_1 of angle α in the overlying thrust sheet as shown in figure 18 (eq 32)

$$S_1 = 2 \tan (^{\circ}\theta_1/2) = \tan \alpha \tag{32}$$

If the overlying thrust sheet contains a crosscutting fault of fundamental-cutoff angle $^{\circ}\theta_2$ prior to imbrication by fault 1, then considering the geometry shown in figure 21A, the new cutoff angle θ'_2 is

$$\theta'_2 = \tan^{-1}\left[\frac{1}{1/\tan {}^{\circ}\theta_2 + 2 \tan (^{\circ}\theta_1/2)}\right] \tag{37}$$

Similarly a third imbrication will have a crosscutting fault of new angle θ'_3

$$\theta'_3 = \tan^{-1}\left[\frac{1}{1/\tan {}^{\circ}\theta_3 + 2 \tan [^{\circ}\theta_1 + \theta'_2)/2]}\right] \tag{38}$$

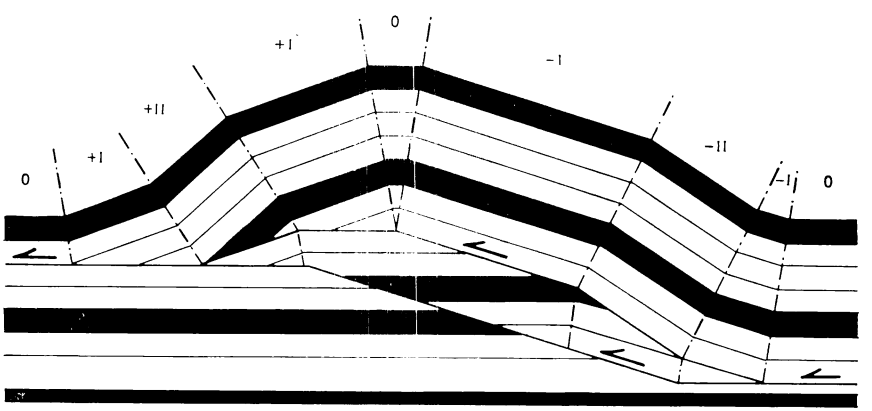

Fig. 20. Panels of forward and back dip in a simple-step fault-bend fold with two imbrications of $\theta = \phi = 18°$ (modfied from Suppe, 1980b).

and the nth imbrication will have a crosscutting fault of new angle θ'_n

$$\theta'_n = \tan^{-1}\left[\frac{1}{1/\tan {}^\circ\theta_n + 2\tan\left[{}^\circ\theta_1 + \theta'_2 + \ldots \theta'_{n-1})/2\right]}\right] \quad (39)$$

Therefore if we know the fundamental cutoff angles ${}^\circ\theta_1$, ${}^\circ\theta_2$, . . . ${}^\circ\theta_n$ we can calculate the back dips associated with each of the n imbrications. This is done for ${}^\circ\theta_1 = {}^\circ\theta_2 = {}^\circ\theta_7$ in table 1.

Forward dips associated with imbrication.—The key to computing the forward dip angle associated with imbrication is certain angular equivalences illustrated in figure 21B. The β-angle of a first or earlier imbrication (β_1, θ_1, ϕ_1) is the θ-angle when it is refolded by a second or later imbrication, for example

$$\beta_1 = \theta_{12} \quad (40)$$

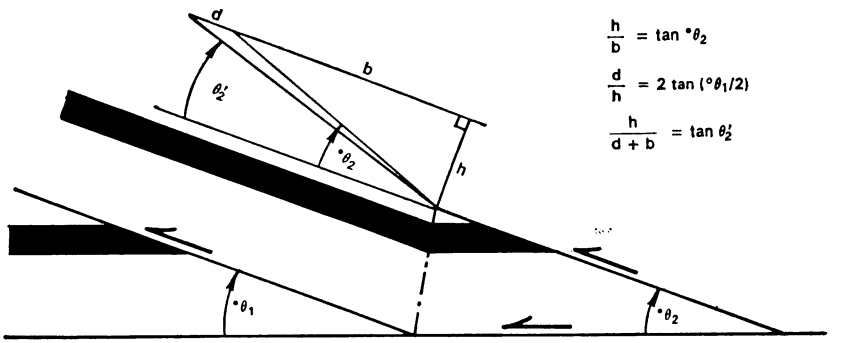

A.

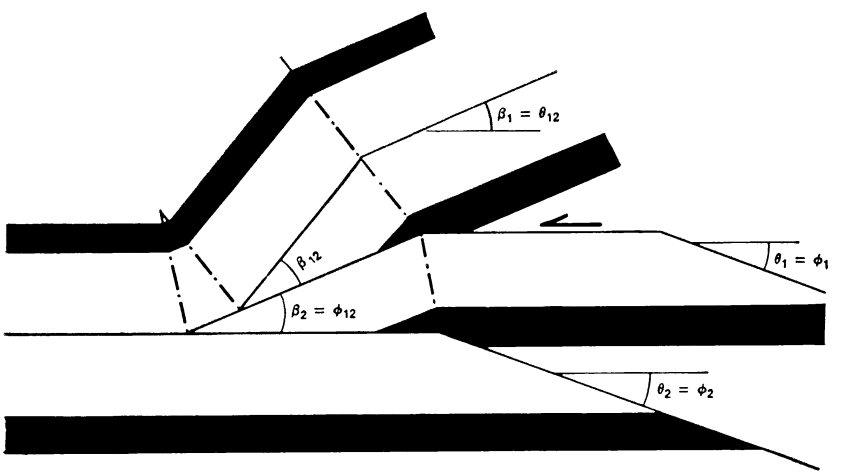

B.

Fig. 21. Angular relationships used in computing the back dips (A) and foreward dips (B) caused by thrust imbrication.

TABLE 1

Forward and Back Dips assuming constant fundamental cutoff angle

Forward Dips							Fundamental	Backdips						
VII	VI	V	IV	III	II	I	Cutoff Angle°θ	I	II	III	IV	V	VI	VII
61.6°	52.5°	43.0°	34.0°	25.2°	16.6°	8.2°	8°	8°	15.9°	23.4°	30.6°	37.3°	43.5°	49.3°
70.2°	59.2°	48.6°	38.3°	28.3°	18.6°	9.2°	9°	9°	17.8°	26.2°	34.0°	41.3°	47.9°	53.9°
80.6°	67.6°	55.2°	43.3°	31.9°	20.9°	10.3°	10°	10°	19.7°	28.9°	37.4°	45.1°	52.0°	58.2°
93.1°	77.3°	62.6°	48.8°	35.7°	23.3°	11.4°	11°	11°	21.6°	31.5°	40.6°	48.7°	55.9°	62.2°
109°	88.8°	71.0°	54.8°	39.8°	25.8°	12.6°	12°	12°	23.5°	34.1°	43.7°	52.1°	59.5°	65.9°
128°	102°	80.5°	61.5°	44.3°	28.5°	13.8°	13°	13°	25.4°	36.7°	46.7°	55.4°	62.9°	69.4°
160°	119°	91.3°	68.6°	48.9°	31.2°	15.0°	14°	14°	27.2°	39.1°	49.5°	58.4°	66.1°	72.5°
—*	146°	104°	76.3°	53.6°	33.9°	16.2°	15°	15°	29.1°	41.5°	52.3°	61.4°	69.0°	75.5°
	—*	124°	85.9°	59.0°	36.8°	17.4°	16°	16°	30.9°	43.9°	54.9°	64.1°	—*	
		—*	99.2°	65.6°	40.2°	18.8°	17°	17°	32.7°	46.2°	57.5°	—*		
		—*	123°	73.1°	43.7°	20.2°	18°	18°	34.4°	48.4°	59.9°	—*		
			—*	82.2°	47.4°	21.6°	19°	19°	36.2°	50.6°	—*			
			—*	97.6°	52.0°	23.2°	20°	20°	37.9°	52.7°	—*			
				—*	57.0°	24.8°	21°	21°	39.6°	—*				
				—*	63.6°	26.6°	22°	22°	41.3°	—*				
				—*	72.0°	28.4°	23°	23°	42.9°	—*				
					—*	30.4°	24°	24°	—*					

* Thinning required in forward dips ($\theta_n = \phi_n > 30°$).

where the subscript 12 indicates the first imbrication folded by the second. Furthermore the β-angle of a second or later imbrication is the fault bend for the folding of a first or earlier imbrication, for example

$$\beta_2 = \phi_{12} \tag{41}$$

The angle of forward dip associated with each of n imbrications may be computed using similar angular relations to those in eqs (40) and (41) and the basic fault-bend fold equations (fig. 7), given the fundamental-cutoff angles $^\circ\theta_1$, $^\circ\theta_2$, . . . $^\circ\theta_n$ associated with each of n simple-step imbrications. This is done for $^\circ\theta_1 = {}^\circ\theta_2 = \ldots {}^\circ\theta_7$ in table 1.

A.

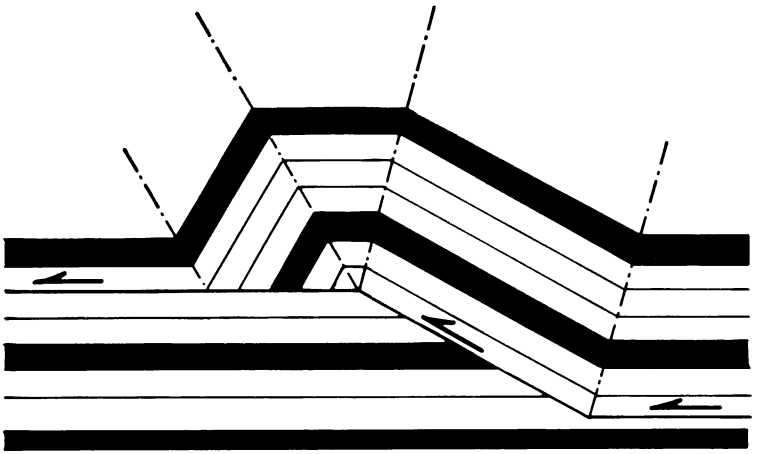

C.

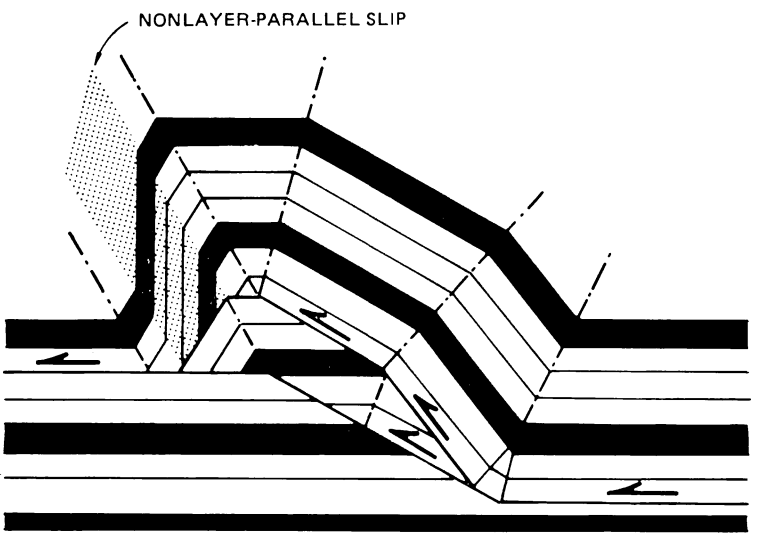

Constant-angle imbrications.—In order to calculate the forward and back dips associated with multiple imbrications we must know the fundamental-cutoff angle $^{\circ}\theta$ for each fault. This procedure is not practical in solving most problems of subsurface geology, unless we have extensive drilling or excellent seismic-reflection profiling. In these problems we generally know the dips in certain regions and wish to solve for the fundamental-cutoff angles, number of imbrications associated with each dip panel (fig. 20), and ultimately the complete spatial arrangement of faults

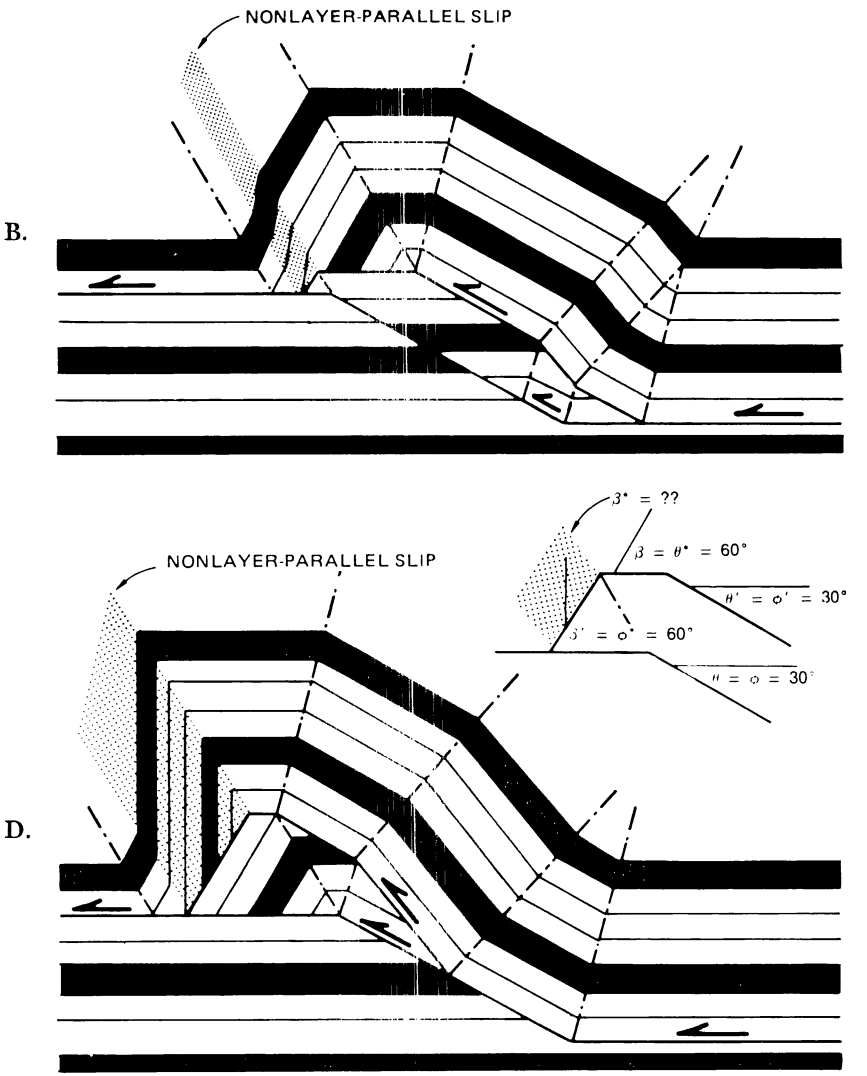

Fig. 22. Non-parallel folding caused by imbricate fault-bend folding with a high fundamental cutoff angle ($\theta = 30°$).

and folds at depth. In many cases we do not have sufficient information to solve the general inverse problem, but the problem may be considerably simplified and made soluble if we are willing to assume that each fault has the same fundamental-cutoff angle $^{\circ}\theta$. This assumption may be mechanically reasonable in that the orientation of stresses relative to bedding may not change greatly between successive imbrications. Furthermore, applications suggest that some imbricate structures obey the constant-angle approximation rather closely.

The angular relations for forward dips are simplified by the constant-angle assumption. Eqs (40) and (41) for example, reduce to

$$\beta_1 = \beta_2 = \theta_{12} = \phi_{12}\,; \tag{42}$$

therefore the refolding of an earlier imbrication by a later imbrication has the geometry of a simple-step in decollement ($\theta = \phi$) and is described by eq (12). The forward and back dips for constant fundamental cutoff angle up to seven imbrications are calculated using eqs (12), (39), and (42) and are presented in table 1.

It should be noted that the folding of an imbrication always involves a fault bend that is larger than the fundamental fault bend, because β is always larger than $\theta = \phi$ for anticlines (fig. 7).

$$\beta > \theta = \phi \qquad \text{for anticlines}\,, \tag{43}$$

and from eq (42) for constant-angle imbrications we have

$$\theta_1 = \phi_1 < \theta_2 = \phi_2 < \ldots \theta_n = \phi_n\,. \tag{44}$$

For imbrications at larger fundamental cutoff angles, refolding may be impossible with conservation of layer thickness because, as we see in figure 7, simple steps of $\theta = \phi$ greater than 30° cannot conserve layer thickness. Therefore, if two faults imbricate at $\phi_1 = \theta_1 = 30°$, as shown in figure 22, the refolding is impossible without change in layer thickness because $\beta_1 = \phi_2 = \theta_2 = 60°$. The maximum fundamental cutoff angle is $\phi = \theta = 23.79°$ for two imbrications conserving layer thickness. The maximum angle is about 20° for three imbrications, 18° for four imbrications, 16° for five imbrications, 15° for six imbrications, and 14° for seven imbrications (table 1). This result emphasizes the importance of observing layer thickness around imbricate fault-bend folds. If layer thickness is conserved then either the fundamental cutoff angle is less than about 20 degrees or some parts of the thrust sheets have undergone additional shear of the sort shown in figure 17.

It is important to realize that the surface shape of an anticline produced by two or more imbrications depends greatly on the amount of slip on each imbrication and on the spacing of the imbrications. A considerable variety of fold shapes can be produced by the mechanism of imbricate fault-bend folding. For example the imbricate structures in figures 23B, C, and D all have exactly the same fault slip and differ only in the distance between the two thrusts. In particular, compare examples B and C with example D; in B and C there is a steepening of forward dips by folding of the first imbrication whereas there is a flattening of forward

dips in example D. We note that in D none of the dip angles differs from a single fault step. Only the short flat segment within the forward dips gives any real hint of imbricate structure at depth. Further slip on the faults of D will, however, produce the steeper dips characteristic of two imbrications.

When there are three or more imbrications substantially more complex geometric relationships exist between surface structure and underlying faults; in these cases stacked anticlines will occur. The complexity

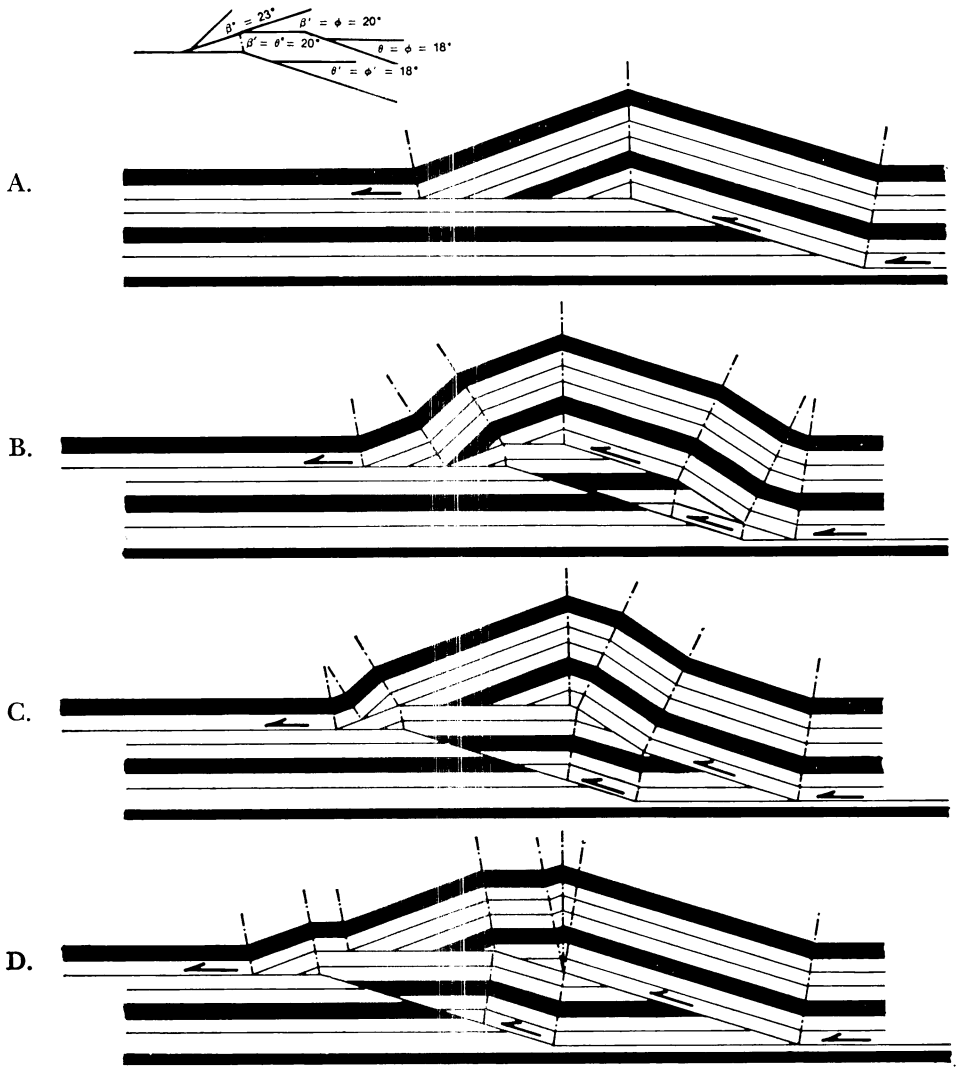

Fig. 23. Illustration of the effect of change in fault spacing on fold shape. Both imbrications have identical slip and cutoff angle. (after Suppe, 1980b).

of the problem of predicting subsurface structure is considerably reduced if we consider the angular relationships between the panels of forward and back dip before we attempt to solve the spatial aspects such as the locations of faults and folds at depth. We call the analysis of angular relations among dip data, *dip-spectral analysis.* This topic is treated in the following section.

Dip-spectral analysis of imbricate structures.—The quantum increase in forward and back dip of each successive imbrication is not a constant for a given fundamental-cutoff angle $^{\circ}\theta$. The quantum change in forward dip becomes larger with each additional imbrication because β is always greater than θ (eq 43). In contrast the quantum change in back dip decreases with each additional imbrication because of shear within the thrust sheets (eqs 32 and 39). Therefore a distinctive and unique spectrum of forward and back dips is associated with each fundamental cutoff angle. For example three imbrications of $^{\circ}\theta = 16^{\circ}$ will produce forward dips of 17°, 37°, and 59° and back dips of 16°, 31°, and 44°, whereas imbrications of $^{\circ}\theta = 14^{\circ}$ will produce forward dips of 15°, 31°, and 49° and back dips of 14°, 27°, and 39°. Note that the forward-dip spectrum is a particularly sensitive indicator of fundamental cutoff angle. If dip data are available from surface mapping, seismic data, or dipmeter surveys, the observed and theoretical spectra can be compared. If the observed structure closely approximates the constant-angle assumption then we can estimate both the fundamental-cutoff angle and number of imbrications associated with each panel of forward and back dips.

The initial steps in producing structural interpretations are (1) assembly of data on a depth section, (2) dip-spectral analysis and assignment of regions of the cross section to the model dips predicted by the dip-spectral analysis, (3) construction of axial surfaces by bisecting the folds ($\gamma_1 = \gamma_2$). At this stage in the analysis any missing information may be noted and assumed or obtained by new measurements.

The next steps in producing structural solutions are substantially more difficult, because they involve guessing a solution and attempting to draw it. This step involves experience and intuition and is an integral part of all methods of subsurface structural interpretation. Nevertheless, it is in a sense more demanding using the present theory because bad guesses are quickly shown to be geometrically impossible. Two examples are given below, based on outcrop and well data from the Appalachians and Taiwan.

Pine Mountain Thrust (fig. 2).—The completed cross section of the Pine Mountain Thrust in the southern Appalachians was already presented in figure 2. We now outline how the structural interpretation was produced. The basic data include detailed surface mapping (England and others, 1961; Harris, 1962) and a well. Dip analysis suggests a fundamental cutoff angle of $^{\circ}\theta = 15^{\circ}$ with an essentially flat regional dip, in agreement with mapping to the west and nearby seismic data of Tegland (1978). The regions of the cross section were assigned to model forward and back dips based on the dip-spectral analysis. The inclinations of the axial surfaces

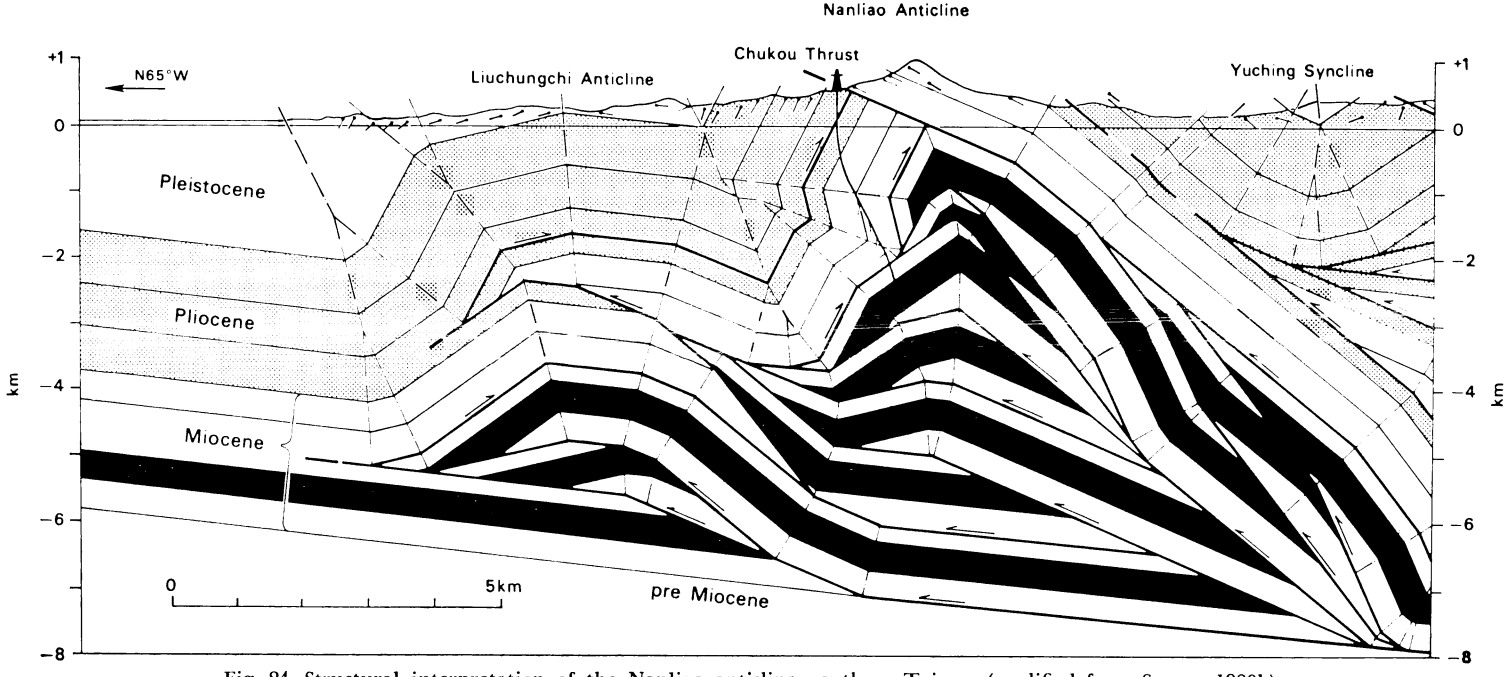

Fig. 24. Structural interpretation of the Nanliao anticline, southern Taiwan (modified from Suppe, 1980b).

are computed using the equal axial angle relationship ($\gamma_1 = \gamma_2$). The positions of some axial surfaces are much better located than others. These positions are adjusted by trial-and-error constrained by stratigraphic thickness and conservation of bed length. The Brooks well encountered the Pine Mountain Thrust below the Cambrian Rome Formation and entered flat-lying Silurian in the footwall. This footwall is elevated relative to the normal formation depths based on drilling and mapping to the west of the section; the normal depth of the Pine Mountain Thrust along the Silurian-Devonian decollement is shown on the left side of figure 2.

Next we must guess a qualitative structural solution. We choose a two imbrication structure based on the minimum of two imbrications deduced from the dip analysis. We choose a solution similar to the theoretical cross section in figure 20. The primary piece of information we do not directly have is the undeformed depth of the Rome décollement; we have two constraints: (1) the stratigraphic thicknesses observed and (2) the positions of axial surfaces. The axial surface east of the Wallen Valley thrust is particularly important, because, as seen in the theoretical cross section (fig. 20), it is the axial surface produced by the footwall cutoff of the Rome Formation along the Pine Mountain Thrust (see fig. 2). The cross section may now be constructed along the lines of figure 20. After some adjustment of positions of axial surfaces by trial and error we arrive at the final solution shown in figure 2.

Nanliao Anticline (fig. 24).—We now consider a much more complex and less well constrained cross section, the Nanliao anticline in western Taiwan (Suppe, 1980b). The basic constraints are the stratigraphic thicknesses, positions of axial surfaces, and surface and well dips. Based on the dip analysis we choose a fundamental-cutoff angle of 18° with a minimum of four imbrications. The regional dip of 6° is known from seismic and well data to the west. The next step in the interpretation was assignment of model dips and provisional location of axial surfaces. The only observed fault is the outcropping Chukou thrust which rides on a decollement in the upper plate. The deeper and higher decollement horizons used in the solution are approximately in positions of decollement in nearby structures. The final solution was then obtained by trial and error using the same methods as the Pine Mountain Thrust.

The proposed solution is obviously not well constrained in light of the uncertain positions of the decollement horizons and the large number of required imbrications. Nevertheless, it provides considerable insight into the structures that may be encountered in further exploration. In particular, the possible existence of structurally stacked reservoirs in the Nanliao anticline is identified by this analysis.

ACKNOWLEDGMENTS

I am indebted to many individuals for their important contributions to this study including J. Bialkowski, Stanley S. L. Chang, C. S. Ho, J. Namson, C. H. Tang, and Y. Wang. I thank D. Elliott, H. P. Laubscher, J. Rodgers, R. Stanley, and R. C. Vierbuchen for reviewing various versions of this manuscript. The subsurface interpretations are based largely

on data generously provided by the Taiwan Petroleum Exploration Division, Chinese Petroleum Corporation. I am grateful to the Chinese Petroleum Corporation, Mining Research and Service Organization, and National Taiwan University for kind hospitality. This work was supported by N.S.F. grant EAR79-25446, "Geometric and Kinematic Properties of Map-scale Decollement Folds." I am grateful to the John Simon Guggenheim Memorial Foundation for gracious and unencumbered support in 1978-1979 during the initial development of these theories.

References

Douglas, R. J. W., 1950, Callum Creek, Langford Creek, and Gap map areas, Alberta: Canada Geol. Survey, Mem. 255, 124 p.

Englund, K. J., Smith, H. L., Harris, L. D., and Stephens, J. G., 1961, Geology of the Ewing Quadrangle, Kentucky and Virginia (1:24,000): U.S. Geol. Survey Map GQ-172.

Gwinn, V. E., 1970, Kinematic patterns and estimates of lateral shortening, Valley and Ridge and Great Valley Provinces, Central Appalachians, South-Central Pennsylvania, *in* Fisher, G. W., Pettijohn, F. J., Reed, V. C., Jr., and Weaver, K. N., eds., Studies of Appalachian Geology: Central and Southern: New York, John Wiley & Sons, p. 127-146.

Harris, L. D., 1962, Geology of the Coleman Gap Quadrangle, Tennessee and Virginia (1:24,000): U.S. Geol. Survey Map GQ-188.

———— 1970, Details of thin-skinned tectonics in parts of Valley and Ridge and Cumberland Plateau provinces of the southern Appalachians, *in* Fisher, G. W., Pettijohn, F. J., Reed, V. C., Jr., and Weaver, K. N., eds., Studies of Appalachian Geology: Central and Southern: New York, John Wiley & Sons, p. 161-173.

Laubscher, H. P., 1965, Ein Kinematisches Modell der Jurafaltung: Ecologae Geol. Helvetiae, no. 58, p. 231-318.

———— 1975, Viscous components in Jura folding: Tectonophysics, v. 27, p. 239-254.

———— 1976, Geometrical adjustments during rotation of a Jura fold limb: Tectonophysics, v. 36, p. 347-365.

Namson, J., 1981, Detailed structural analysis of the western foothills belt in the Miaoli-Hsinchu area, Taiwan: I. southern part: Petroleum Geology of Taiwan, no. 18, p. 31-51.

Perry, W. J., Harris, A. G., and Harris, L. D., 1979, Conodont-based reinterpretation of Bain Dome—Structural reevaluation of Allegheny frontal zone: Am. Assoc. Petroleum Geologists Bull., v. 63, p. 647-675.

Rich, J. L., 1934, Mechanics of low-angle overthrust faulting as illustrated by Cumberland thrust block, Virginia, Kentucky, and Tennessee: Am. Assoc. Petroleum Geologists Bull., v. 18, p. 1584-1596.

Rodgers, John, 1950, Mechanics of Appalachian folding as illustrated by Sequatchie anticline, Tennessee and Alabama: Am. Assoc. Petroleum Geologists Bull., v. 34, p. 672-681.

Roedder, D., Gilbert, O. E., Jr., and Witherspoon, W. D., 1978, Evolution and macroscopic structure of valley and ridge thrust belt, Tennessee and Virginia: Knoxville, Univ. Tennessee Dept. Geol. Sci., Studies in Geology, no. 2, 25 p.

Suppe, John, 1976, Decollement folding in western Taiwan: Petroleum Geology Taiwan, no. 13, p. 25-35.

———— 1979, Fault bend folding (abstract): Geol. Soc. America Abs. with Programs, v. 11, p. 525.

———— 1980a, A retrodeformable cross section of northern Taiwan: Geol. Soc. China Proc., no. 23, p. 46-55.

———— 1980b, Imbricated structure of western foothills belt, south-central Taiwan: Petroleum Geology Taiwan, no. 17, p. 1-16.

———— 1981, Mechanics of mountain building and metamorphism in Taiwan: Geol. Soc. China, Mem. 4, p. 67-89.

Suppe, John, and Namson, J., 1979, Fault-bend origin of frontal folds of the western Taiwan fold-and-thrust belt: Petroleum Geology Taiwan, no. 16, p. 1-18.

Tegland, E. R., 1978, Seismic investigations of eastern Tennessee: Tennessee Div. Geology Bull., no. 78, 68 p.